10

Homogeneous, Isotropic Cosmology

10.1 Observational basis

Since 1998, observations have converged on a **Standard "ΛCDM" Model of Cosmology**, a spatially flat Universe dominated by gravitationally repulsive dark energy whose equation of state is consistent with that of a cosmological constant (Λ), and by gravitationally attractive non-baryonic cold dark matter (CDM). The mass-energy of the Standard Model of the Universe consists of 72% dark energy, 24% CDM, 4.6% baryonic matter, and a sprinkling of photons and neutrinos. The designation "baryonic" is conventional but misleading: it refers to all atomic matter, including not only baryons (nuclei), but also non-relativistic leptons (electrons).

10.1.1 The expansion of the Universe

The **Hubble diagram**, a diagram of distance versus redshift of distant astronomical objects, indicates that the Universe is expanding.

Hubble's law states that galaxies are receding with velocity proportional to distance, $v = H_0 d$, with constant of proportionality the Hubble constant H_0 (the 0 subscript signifies the present day value). Hubble's law was first proposed by Georges Lemaître (1927) and by Edwin Hubble (1929) on the basis of observations.

The recession velocity v of an astronomical object can be determined with some precision from the redshift of its spectral lines, but its distance d is more difficult to measure, because astronomical objects, such as galaxies, typically have a wide range of intrinsic luminosities. Hubble estimated distances to galaxies using Cepheid variable stars, which had been discovered by Henrietta Leavitt (1912) to have periods proportional to their luminosities. A good distance estimator should be a "standard candle" of predictable luminosity, and it should be bright, so that it can be seen over cosmological distances.

The best modern Hubble diagram is that of Type Ia supernovae, illustrated in Figure 10.1, adapted from Conley et al. (2011). A Type Ia supernova is thought to represent the thermonuclear explosion of a white dwarf star that through accretion from a companion star reaches the Chandrasekhar mass limit of $1.4\,\mathrm{M}_\odot$. Having a similar origin, such supernovae approximate standard candles (or standard bombs) having the same luminosity. Actually, some variation in luminosity is observed, which can be attributed to the amount of

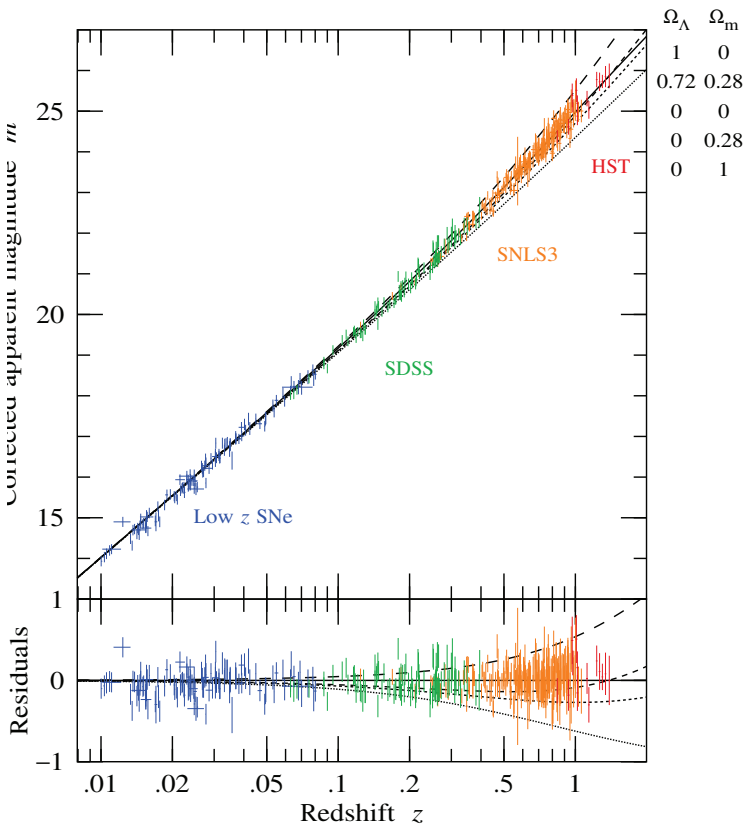

Figure 10.1 Hubble diagram of 472 Type Ia supernovae from a compilation of surveys, adapted from Conley et al. (2011). The vertical axis is the apparent magnitude m (= apparent brightness) of the supernova, with an empirical correction based on the shape of its lightcurve. The various smooth curves are 5 theoretical model Hubble diagrams, with parameters from top to bottom as indicated at top right. The solid line is a flat ΛCDM model with $\Omega_\Lambda = 0.72$ and $\Omega_\mathrm{m} = 0.28$. The bottom panel shows residuals.

^{56}Ni synthesized in the explosion, and which can be corrected at least in part through an empirical relation between luminosity and how rapidly the lightcurve decays (higher luminosity supernovae decay more slowly).

10.1.2 The acceleration of the Universe

Since light takes time to travel from distant parts of the Universe to astronomers here on Earth, the higher the redshift of an object, the further back in time astronomers are seeing.

In 1998 two teams, the Supernova Cosmology Project (Perlmutter, 1999), and the High-z Supernova Search team (Riess and Filippenko, 1998), precipitated the revolution that led to the Standard Model of Cosmology. They reported that observations of Type Ia supernova at high redshift indicated that the Universe is not only expanding, but also accelerating. The acceleration requires the mass-energy density of the Universe to be dominated at the present time by a gravitationally repulsive component, such as a cosmological constant Λ.

In the Hubble diagram of Type Ia supernova shown in Figure 10.1, the fitted curve is a best-fit flat cosmological model containing a cosmological constant and matter.

10.1.3 The Cosmic Microwave Background (CMB)

The single most powerful observational constraints on the Universe come from the Cosmic Microwave Background (CMB). Modern observations of the CMB have ushered in an era of precision cosmology, where key cosmological parameters are being measured with percent level uncertainties.

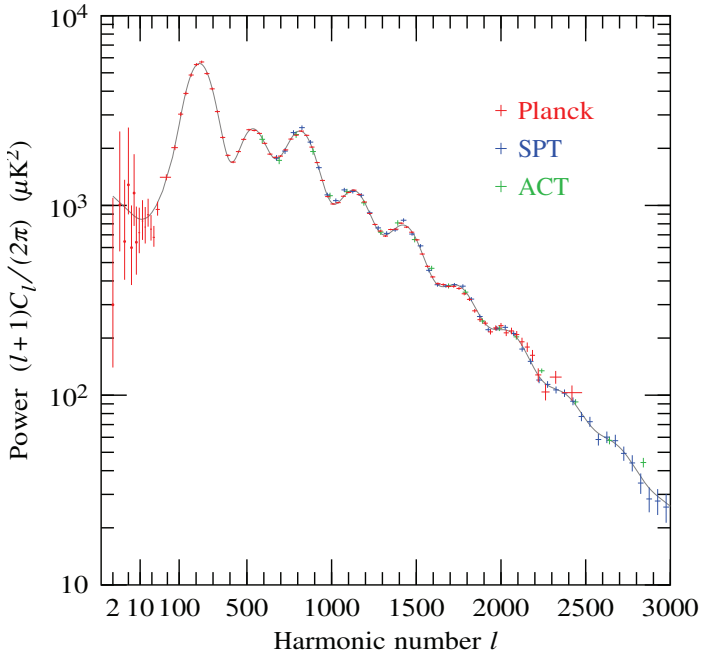

Figure 10.2 Power spectrum of fluctuations in the CMB from observations with the Planck satellite (Ade, 2013), the South Pole Telescope (Keisler and Reichardt, 2011), and the Atacama Cosmology Telescope (Das and Sherwin, 2011). The plot is logarithmic in harmonic number l up to 100, linear thereafter. The fit is a best-fit flat ΛCDM model.

The CMB was discovered serendipitously by Arno Penzias & Robert Wilson (1965), who were puzzled by an apparently uniform excess temperature from a horn antenna, 6 meters in size, tuned to a wavelength of $\sim 7\,\mathrm{cm}$, that they had built to detect radio waves. They were unaware that Robert Dicke's group at Princeton had already realized that a hot Big Bang would have left a remnant of blackbody radiation filling the Universe, with a present-day temperature of a few Kelvin, and were setting about to try to detect it. When Penzias heard about Dicke's work, he and Wilson quickly realized that their observations fit what the Princeton group were predicting. The observations of Penzias and Wilson (1965) were published along with a theoretical explanation by Dicke et al. (1965) in back-to-back papers in an issue of the Astrophysical Journal Letters.

Dicke et al. (1965) argued that the temperature of the expanding Universe must have been higher in the past, and there must have been a time before which the temperature was high enough to ionize hydrogen, about 3,000 K. Before this time, called recombination, hydrogen and other elements would have been mostly ionized. The CMB comes to us from the time of recombination, when the Universe transitioned from being mainly ionized, and therefore opaque, to being mainly neutral, and therefore transparent. Recombination occurred when the Universe was about 400,000 years old, and the CMB has streamed essentially freely through the Universe since that time. Thus the CMB provides a snapshot of the Universe at recombination.

The CMB spectrum peaks in microwaves, which are absorbed by water vapour in the atmosphere. Modern observations of the CMB are therefore made using satellites, or with balloons, or at high-altitude sites with low water vapour, such as the South Pole, or the Atacama Desert in Chile.

The characteristics of the CMB measured from modern observations are as follows.

The CMB has a remarkably precise black body spectrum with temperature $T_0 = 2.72548 \pm 0.00057\,\mathrm{K}$ (Fixsen, 2009).

The CMB shows a dipole anisotropy of $\Delta T = 3.355 \pm 0.008\,\mathrm{mK}$, implying that the solar system is moving at velocity $v = 369.1\,\mathrm{km\,s^{-1}}$ through the CMB in the Galactic coordinate direction $\{l, b\} = \{263.^{\circ}99 \pm 0.14, 48.^{\circ}26 \pm 0.03\}$ (Jarosik et al., 2011).

After dipole subtraction, the temperature of the CMB over the sky is uniform to a few parts in 10^5.

The power spectrum of temperature T fluctuations shows a scale-invariant spectrum at large scales, and prominent acoustic peaks at smaller scales, Figure 10.2. The power spectrum fits astonishingly well to predictions based on the theory of inflation, §10.22, in its simplest form. The power spectrum yields precision measurements of some basic cosmological parameters, notably the densities of the principal contributions to the energy-density of the Universe: dark energy, non-baryonic cold dark matter, and baryons.

Fluctuations in the CMB are expected to be polarized at some level. There are two independent modes of polarization, "E" (divergence) modes and "B" (curl) modes. There are corresponding E-mode and B-mode power spectra. Of the cross-power spectra between temperature T and E and B fluctuations, only the T–E cross-power is expected to be non-vanishing. The T–E cross-power spectrum has been measured by the WMAP satellite, and is interpreted as arising from scattering of CMB photons by ionized gas intervening between recombination and us.

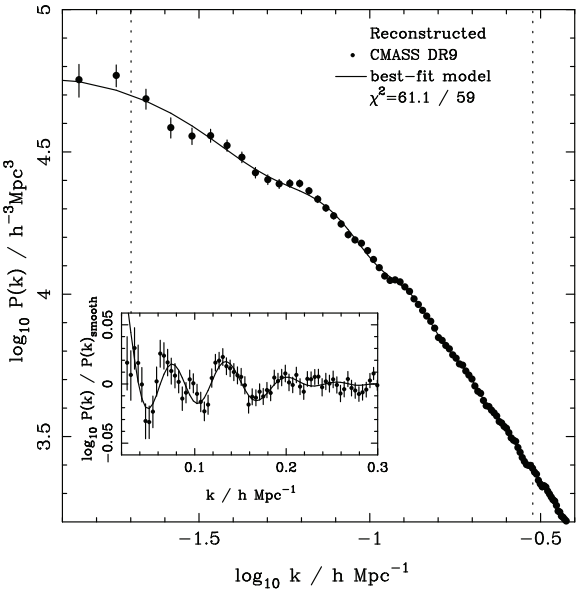

Figure 10.3 Power spectrum of galaxies from the Baryon Oscillation Spectroscopic Survey (BOSS), which is part of the Sloan Digital Sky Survey III (SDSS-III) (Anderson, 2013). The survey contains 264,283 massive galaxies, covering 3,275 square degrees. The inset shows the spectrum with a smooth component subtracted to bring out the baryon acoustic oscillations (BAO). The fitted curve is a flat ΛCDM model.

10.1.4 The clustering of galaxies

The clustering of galaxies shows a power spectrum in good agreement with the Standard Model, Figure 10.3.

Historically, the principal evidence for non-baryonic cold dark matter was comparison between the power spectra of galaxies versus CMB. How can tiny fluctuations in the CMB grow into the observed fluctuations in matter today in only the age of the Universe? The answer was, non-baryonic dark matter that begins to cluster before recombination, when the CMB was released.

The interpretaton of the power spectrum of galaxies is complicated by the facts that galaxies have undergone non-linear clustering at smaller scales, and that galaxies are a biassed tracer of mass. However, the pattern of clustering at large, linear scales retains an imprint of baryonic acoustic oscillations (BAO) analogous to those in the CMB. Observations from large galaxy surveys have been able to detect the predicted BAO, Figure 10.3. Comparison of the scales of acoustic oscillations in galaxies and the CMB allows the two scales to be matched, pinning the relative scales of galaxies today with those in the CMB at redshift $z \sim 1000$.

Major plans are underway to measure galaxy clustering as a function of redshift, with the primary aim to determine whether the evolution of dark energy is consistent with that of a cosmological constant. Such a

measurement cannot be done with CMB observations, since the CMB offers only a snapshot of the Universe at high redshift.

10.1.5 Other supporting evidence

- The observed abundances of light elements H, D, ^{3}He, He, and Li are consistent with the predictions of big bang nucleosynthesis (BBN) provided that the baryonic density is $\Omega_{\rm b} \approx 0.04$, in good agreement with measurements from the CMB.
- The ages of the oldest stars, in globular clusters, agree with the age of the Universe with dark energy, but are older than the Universe without dark energy.
- The existence of dark matter, possibly non-baryonic, is supported by ubiquitous evidence for unseen dark matter, deduced from sizes and velocities (or in the case of gravitational lensing, the gravitational potential) of various objects:
  - The Local Group of galaxies;
  - Rotation curves of spiral galaxies;
  - The temperature and distribution of x-ray gas in elliptical galaxies, and in clusters of galaxies;
  - Gravitational lensing by clusters of galaxies.
- The abundance of galaxy clusters as a function of redshift is consistent with a matter density $\Omega_{\rm m} \approx 0.3$, but not much higher. A low matter density slows the gravitational clustering of galaxies, implying relatively more and richer clusters at high redshift than at the present, as observed.
- The Bullet cluster is a rare example that supports the notion that the dark matter is non-baryonic. In the Bullet cluster, two clusters recently passed through each other. The baryonic matter, as measured from x-ray emission of hot gas, appears displaced from the dark matter, as measured from weak gravitational lensing.

10.2 Cosmological Principle

The **cosmological principle** states that the Universe at large is
- **homogeneous** (has spatial translation symmetry),
- **isotropic** (has spatial rotation symmetry).

The primary evidence for this is the uniformity of the temperature of the CMB, which, after subtraction of the dipole produced by the motion of the solar system through the CMB, is constant over the sky to a few parts in 10^5. Confirming evidence is the statistical uniformity of the distribution of galaxies over large scales.

The cosmological principle allows that the Universe evolves in time, as observations surely indicate — the Universe is expanding, galaxies, quasars, and galaxy clusters evolve with redshift, and the temperature of the CMB has undoubtedly decreased since recombination.

10.3 Friedmann-Lemaître-Robertson-Walker metric

Universes satisfying the cosmological principle are described by the Friedmann-Lemaître-Robertson-Walker (FLRW) metric, equation (10.26) below, discovered independently by Friedmann (1922) and Friedmann (1924), and Lemaître (1927). (English translation in Lemaître 1931). The FLRW metric was shown to be the unique metric for a homogeneous, isotropic universe by Robertson (1935), Robertson (1936a), and Robertson (1936b) and Walker (1937). The metric, and the associated Einstein equations, which are known as the Friedmann equations, are set forward in the next several sections, §§10.4–10.9.

10.4 Spatial part of the FLRW metric: informal approach

The cosmological principle implies that

$$\boxed{\text{the spatial part of the FLRW metric is a 3D hypersphere}} \ . \tag{10.1}$$

In this context the term hypersphere is to be construed as including not only cases of positive curvature, which have finite positive radius of curvature, but also cases of zero and negative curvature, which have infinite and imaginary radius of curvature.

Figure 10.4 shows an embedding diagram of a 3D hypersphere in 4D Euclidean space. The horizontal directions in the diagram represent the normal 3 spatial x, y, z dimensions, with one dimension z suppressed, while the vertical dimension represents the 4th spatial dimension w. The 3D hypersphere is a set of points $\{x, y, z, w\}$ satisfying

$$\left(x^2 + y^2 + z^2 + w^2\right)^{1/2} = R = \text{constant} \ . \tag{10.2}$$

An observer is sitting at the north pole of the diagram, at $\{0, 0, 0, 1\}$. A 2D sphere (which forms a 1D circle in the embedding diagram of Figure 10.4) at fixed distance surrounding the observer has **geodesic distance** $r_\parallel$ defined by

$$r_\parallel \equiv \text{proper distance to sphere measured along a radial geodesic} \ , \tag{10.3}$$

and **circumferential radius** r defined by

$$r \equiv \left(x^2 + y^2 + z^2\right)^{1/2} \ , \tag{10.4}$$

which has the property that the proper circumference of the sphere is $2\pi r$. In terms of $r_\parallel$ and r, the spatial metric is

$$dl^2 = dr_\parallel^2 + r^2 do^2 \ , \tag{10.5}$$

where $do^2 \equiv d\theta^2 + \sin^2\theta \, d\phi^2$ is the metric of a unit 2-sphere.

Introduce the angle χ illustrated in the diagram. Evidently

$$\begin{aligned} r_\parallel &= R\chi \ , \\ r &= R \sin\chi \ . \end{aligned} \tag{10.6}$$

In terms of the angle χ, the spatial metric is

$$dl^2 = R^2 \left(d\chi^2 + \sin^2\chi \, do^2 \right) \ , \tag{10.7}$$

which is one version of the spatial FLRW metric. The metric resembles the metric of a 2-sphere of radius R, which is not surprising since the same construction, with Figure 10.4 interpreted as the embedding diagram of a 2D sphere in 3D, yields the metric of a 2-sphere. Indeed, the construction iterates to give the metric of an N-dimensional sphere of arbitrarily many dimensions N.

Instead of the angle χ, the metric can be expressed in terms of the circumferential radius r. It follows from equations (10.6) that

$$r_\parallel = R \sin^{-1}(r/R) \ , \tag{10.8}$$

whence

$$\begin{aligned} dr_\parallel &= \frac{dr}{\sqrt{1 - r^2/R^2}} \\ &= \frac{dr}{\sqrt{1 - Kr^2}} \ , \end{aligned} \tag{10.9}$$

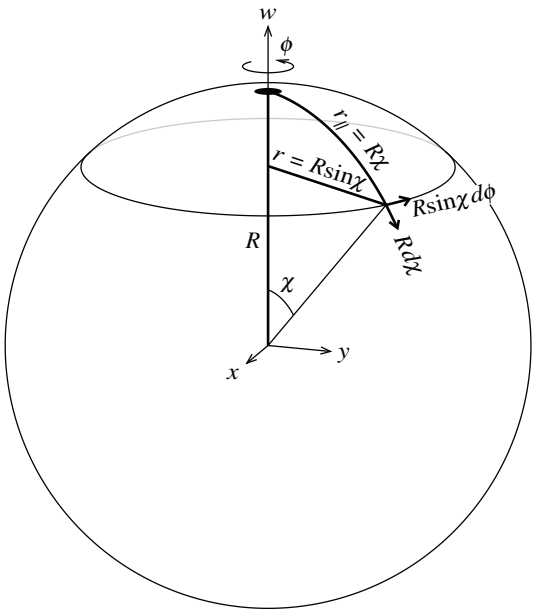

Figure 10.4 Embedding diagram of the FLRW geometry.

where K is the curvature

$$K \equiv \frac{1}{R^2} \ . \tag{10.10}$$

In terms of r, the spatial FLRW metric is then

$$\boxed{dl^2 = \frac{dr^2}{1 - Kr^2} + r^2 do^2} \ . \tag{10.11}$$

The embedding diagram Figure 10.4 is a nice prop for the imagination, but it is not the whole story. The curvature K in the metric (10.11) may be not only positive, corresponding to real finite radius R, but also zero or negative, corresponding to infinite or imaginary radius R. The possibilities are called closed, flat, and open:

$$K \begin{cases} > 0 & \text{closed} & R \text{ real} \ , \\ = 0 & \text{flat} & R \to \infty \ , \\ < 0 & \text{open} & R \text{ imaginary} \ . \end{cases} \tag{10.12}$$

10.5 Comoving coordinates

The metric (10.11) is valid at any single instant of cosmic time t. As the Universe expands, the 3D spatial hypersphere (whether closed, flat, or open) expands. In cosmology it is highly advantageous to work in **comoving coordinates** that expand with the Universe. Why? Firstly, it is helpful conceptually and mathematically to think of the Universe as at rest in comoving coordinates. Secondly, linear perturbations, such as those in the CMB, have wavelengths that expand with the Universe, and are therefore fixed in comoving coordinates.

In practice, cosmologists introduce the **cosmic scale factor** $a(t)$

$$a(t) \equiv \text{measure of the size of the Universe, expanding with the Universe} \ , \tag{10.13}$$

which is proportional to but not necessarily equal to the radius R of the Universe. The cosmic scale factor a can be normalized in any arbitrary way. The most common convention adopted by cosmologists is to normalize it to unity at the present time,

$$a_0 = 1 \ , \tag{10.14}$$

where the 0 subscript conventionally signifies the present time.

Comoving geodesic and circumferential radial distances $x_\parallel$ and x are defined in terms of the proper geodesic and circumferential radial distances $r_\parallel$ and r by

$$a x_\parallel \equiv r_\parallel \ , \quad a x \equiv r \ . \tag{10.15}$$

Objects expanding with the Universe remain at fixed comoving positions $x_\parallel$ and x. In terms of the comoving

circumferential radius x, the spatial FLRW metric is

$$\boxed{dl^2 = a^2\left(\frac{dx^2}{1-\kappa x^2} + x^2 do^2\right)}\,, \tag{10.16}$$

where the curvature constant κ, a constant in time and space, is related to the curvature K, equation (10.10), by

$$\kappa \equiv a^2 K\ . \tag{10.17}$$

Alternatively, in terms of the geodesic comoving radius $x_\parallel$, the spatial FLRW metric is

$$dl^2 = a^2\left(dx_\parallel^2 + x^2 do^2\right)\ , \tag{10.18}$$

where

$$x = \begin{cases} \dfrac{\sin(\kappa^{1/2} x_\parallel)}{\kappa^{1/2}} & \kappa > 0 \quad \text{closed}\ , \\ x_\parallel & \kappa = 0 \quad \text{flat}\ , \\ \dfrac{\sinh(|\kappa|^{1/2} x_\parallel)}{|\kappa|^{1/2}} & \kappa < 0 \quad \text{open}\ . \end{cases} \tag{10.19}$$

Actually it is fine to use just the top expression of equations (10.19), which is mathematically equivalent to the bottom two expressions when $\kappa = 0$ or $\kappa < 0$ (because $\sin(ix)/i = \sinh(x)$).

For some purposes it is convenient to normalize the cosmic scale factor a so that $\kappa = 1$, 0, or -1. In this case the spatial FLRW metric may be written

$$dl^2 = a^2\left(d\chi^2 + x^2 do^2\right)\ , \tag{10.20}$$

where

$$x = \begin{cases} \sin(\chi) & \kappa = 1 \quad \text{closed}\ , \\ \chi & \kappa = 0 \quad \text{flat}\ , \\ \sinh(\chi) & \kappa = -1 \quad \text{open}\ . \end{cases} \tag{10.21}$$

10.6 Spatial part of the FLRW metric: more formal approach

A more formal approach to the derivation of the spatial FLRW metric from the cosmological principle starts with the proposition that the spatial components $G_{\alpha\beta}$ of the Einstein tensor at fixed scale factor a (all time derivatives of a set to zero) should be proportional to the metric tensor

$$G_{\alpha\beta} = -K\, g_{\alpha\beta} \quad (\alpha, \beta = 1, 2, 3)\ . \tag{10.22}$$

Without loss of generality, the spatial metric can be taken to be of the form

$$dl^2 = f(r)\, dr^2 + r^2 do^2\ . \tag{10.23}$$

Imposing the condition (10.22) on the metric (10.23) recovers the spatial FLRW metric (10.11).

Exercise 10.1 Isotropic (Poincaré) form of the FLRW metric. By a suitable transformation of the comoving radial coordinate x, bring the spatial FLRW metric (10.16) to the "isotropic" form

$$dl^2 = \frac{4a^2}{\left(1+\kappa X^2\right)^2}\left(dX^2 + X^2 do^2\right) \ . \tag{10.24}$$

What is the relation between X and x?

For an open geometry, $\kappa < 0$, the isotropic line-element (10.24) is also called the Poincaré ball, or in 2D the Poincaré disk, Figure 10.5. By construction, the isotropic line-element (10.24) is conformally flat, meaning that it equals the Euclidean line-element multiplied by a position-dependent conformal factor. Conformal transformations of a line-element preserve angles.

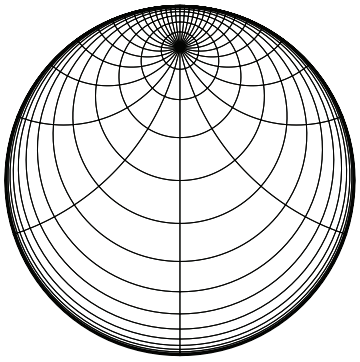

Figure 10.5 The Poincaré disk depicts the geometry of an open FLRW universe in isotropic coordinates. The lines are lines of latitude and longitude relative to a "pole" chosen here to be displaced from the centre of the disk. In isotropic coordinates, geodesics correspond to circles that intersect the boundary of the disk at right angles, such as the lines of constant longitude in this diagram. The lines of latitude remain unchanged under rotations about the pole.

Solution.

$$X = \frac{x}{1+\sqrt{1-\kappa x^2}} = \frac{1}{\sqrt{\kappa}}\tan\left(\frac{\sqrt{\kappa}\,x_\parallel}{2}\right) \ , \quad x = \frac{2X}{1+\kappa X^2} = \frac{1}{\sqrt{\kappa}}\sin\left(\sqrt{\kappa}\,x_\parallel\right) \ . \tag{10.25}$$

For an open geometry with $\kappa = -1$, X goes from 0 to 1 as x goes from 0 to ∞.

10.7 FLRW metric

The full Friedmann-Lemaître-Robertson-Walker spacetime metric is

$$\boxed{ds^2 = -dt^2 + a(t)^2 \left(\frac{dx^2}{1-\kappa x^2} + x^2 do^2 \right)}\,, \tag{10.26}$$

where t is **cosmic time**, which is the proper time experienced by comoving observers, who remain at rest in comoving coordinates $dx = d\theta = d\phi = 0$. Any of the alternative versions of the comoving spatial FLRW metric, equations (10.16), (10.18), (10.20), or (10.24), may be used as the spatial part of the FLRW spacetime metric (10.26).

10.8 Einstein equations for FLRW metric

The Einstein equations for the FLRW metric (10.26) are

$$\begin{aligned} -G^t_t = 3\left(\frac{\kappa}{a^2} + \frac{\dot{a}^2}{a^2}\right) &= 8\pi G\rho\,, \\ G^x_x \;=\; G^\theta_\theta \;=\; G^\phi_\phi = -\frac{\kappa}{a^2} - \frac{\dot{a}^2}{a^2} - \frac{2\,\ddot{a}}{a} &= 8\pi G p\,, \end{aligned} \tag{10.27}$$

where overdots represent differentiation with respect to cosmic time t, so that for example $\dot{a} \equiv da/dt$. Note the trick of one index up, one down, to remove, modulo signs, the distorting effect of the metric on the Einstein tensor. The Einstein equations (10.27) rearrange to give **Friedmann's equations**

$$\boxed{\frac{\dot{a}^2}{a^2} = \frac{8\pi G\rho}{3} - \frac{\kappa}{a^2}}\,, \tag{10.28a}$$

$$\boxed{\frac{\ddot{a}}{a} = -\frac{4\pi G}{3}\,(\rho + 3p)}\,. \tag{10.28b}$$

Friedmann's two equations (10.28) are fundamental to cosmology. The first one relates the curvature κ of the Universe to the expansion rate $\dot{a}/a$ and the density ρ. The second one relates the acceleration $\ddot{a}/a$ to the density ρ plus 3 times the pressure p.

10.9 Newtonian "derivation" of Friedmann equations

The Friedmann equations can be reproduced with a heuristic Newtonian argument.

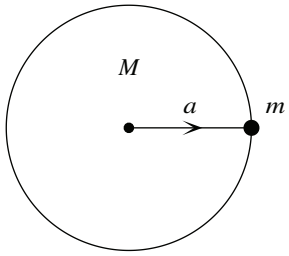

Figure 10.6 Newtonian picture in which the Universe is modeled as a uniform density sphere of radius a and mass M that gravitationally attracts a test mass m.

10.9.1 Energy equation

Model a piece of the Universe as a ball of radius a with uniform density ρ, hence of mass $M = \frac{4}{3}\pi\rho a^3$. Consider a small mass m attracted by this ball. Conservation of the kinetic plus potential energy of the small mass m implies

$$\frac{1}{2}m\dot{a}^2 - \frac{GMm}{a} = -\frac{\kappa mc^2}{2} \ , \tag{10.29}$$

where the quantity on the right is some constant whose value is not determined by this Newtonian treatment, but which GR implies is as given. The energy equation (10.29) rearranges to

$$\boxed{\frac{\dot{a}^2}{a^2} = \frac{8\pi G\rho}{3} - \frac{\kappa c^2}{a^2}} \ , \tag{10.30}$$

which reproduces the first Friedmann equation.

10.9.2 First law of thermodynamics

For adiabatic expansion, the first law of thermodynamics is

$$dE + p\,dV = 0 \ . \tag{10.31}$$

With $E = \rho V$ and $V = \frac{4}{3}\pi a^3$, the first law (10.31) becomes

$$d(\rho a^3) + p\,da^3 = 0 \ , \tag{10.32}$$

or, with the derivative taken with respect to cosmic time t,

$$\dot{\rho} + 3(\rho + p)\frac{\dot{a}}{a} = 0 \ . \tag{10.33}$$

Differentiating the first Friedmann equation in the form

$$\dot{a}^2 = \frac{8\pi G\rho a^2}{3} - \kappa c^2 \tag{10.34}$$

gives

$$2\dot{a}\ddot{a} = \frac{8\pi G}{3}\left(\dot{\rho}a^2 + 2\rho a\dot{a}\right) \ , \tag{10.35}$$

and substituting $\dot{\rho}$ from the first law (10.33) reduces this to

$$2\dot{a}\ddot{a} = \frac{8\pi G}{3}a\dot{a}\left(-\rho - 3p\right) \ . \tag{10.36}$$

Hence

$$\boxed{\frac{\ddot{a}}{a} = -\frac{4\pi G}{3}\left(\rho + 3p\right)} \, , \tag{10.37}$$

which reproduces the second Friedmann equation.

10.9.3 Comment on the Newtonian derivation

The above Newtonian derivation of Friedmann's equations is only heuristic. A different result could have been obtained if different assumptions had been made. If for example the Newtonian gravitational force law $m\ddot{a} = -GMm/a^2$ were taken as correct, then it would follow that $\ddot{a}/a = -\frac{4}{3}\pi G\rho$, which is missing the all-important $3p$ contribution (without which there would be no inflation or dark energy) to Friedmann's second equation.

It is notable that the first law of thermodynamics is built in to the Friedmann equations. This implies that entropy is conserved in FLRW Universes. This remains true even when the mix of particles changes, as happens for example during the epoch of electron-positron annihilation, or during big bang nucleosynthesis. How then does entropy increase in the real Universe? Through fluctuations away from the perfect homogeneity and isotropy assumed by the FLRW metric.

10.10 Hubble parameter

The **Hubble parameter** $H(t)$ is defined by

$$\boxed{H \equiv \frac{\dot{a}}{a}} \, . \tag{10.38}$$

The Hubble parameter H varies in cosmic time t, but is constant in space at fixed cosmic time t.

The value of the Hubble parameter today is called the **Hubble constant** H_0 (the subscript 0 signifies the present time). The Hubble constant measured from Cepheid variable stars and Type Ia supernova is (Riess, Macri, et al., 2011)

$$\boxed{H_0 = 73.8 \pm 2.4 \ \mathrm{km\,s^{-1}\,Mpc^{-1}}} \, . \tag{10.39}$$

The WMAP CMB power spectrum by itself gives only weak constraints on H_0, but the recent addition of

high harmonic data, Figure **??**, permits an independent measurement of H_0 from CMB data alone (Hinshaw et al., 2012), UPDATE TO PLANCK

$$H_0 = 71 \pm 7 \text{ km s}^{-1} \text{ Mpc}^{-1} \ . \tag{10.40}$$

Baryonic Acoustic Oscillations (BAO) measured from the power spectrum of galaxies, Figure 10.3, yield an independent measure of scale. From a combination of the direct measurement of H_0 with BAO and CMB measurements, Hinshaw et al. (2012) find

$$H_0 = 69 \pm 1 \text{ km s}^{-1} \text{ Mpc}^{-1} \ . \tag{10.41}$$

The distance d to an object that is receding with the expansion of the universe is proportional to the cosmic scale factor, $d \propto a$, and its recession velocity v is consequently proportional to $\dot{a}$. The result is **Hubble's law** relating the recession velocity v and distance d of distant objects

$$\boxed{v = H_0 d} \ . \tag{10.42}$$

Since it takes light time to travel from a distant object, and the Hubble parameter varies in time, the linear relation (10.42) breaks down at cosmological distances.

We, in the Milky Way, reside in an overdense region of the Universe that has collapsed out of the general Hubble expansion of the Universe. The local overdense region of the Universe that has just turned around from the general expansion and is beginning to collapse for the first time is called the **Local Group** of galaxies. The Local Group consists of order 100 galaxies, mostly dwarf and irregular galaxies. It contains two major spiral galaxies, Andromeda (M31) and the Milky Way, and one mid-sized spiral galaxy Triangulum (M33). The Local Group is about 1 Mpc in radius.

Because of the ubiquity of the Hubble constant in cosmological studies, cosmologists often parameterize it by the quantity h defined by

$$h \equiv \frac{H_0}{100 \text{ km s}^{-1} \text{ Mpc}^{-1}} \ . \tag{10.43}$$

The reciprocal of the Hubble constant gives an approximate estimate of the age of the Universe (c.f. Exercise 10.6),

$$\frac{1}{H_0} = 9.778 \, h^{-1} \text{ Gyr} = 14.2 \, h_{0.69}^{-1} \text{ Gyr} \ . \tag{10.44}$$

10.11 Critical density

The critical density $\rho_{\rm crit}$ is defined to be the density required for the Universe to be flat, $\kappa = 0$. According to the first of Friedmann equations (10.28), this sets

$$\boxed{\rho_{\rm crit} \equiv \frac{3H^2}{8\pi G}} \ . \tag{10.45}$$

The critical density $\rho_{\rm crit}$, like the Hubble parameter H, evolves with time.

Table 10.1 *Cosmic inventory*

Species		Hinshaw et al. (2012)
Dark energy (Λ)	Ω_Λ	0.72 ± 0.01
Non-baryonic cold dark matter (CDM)	Ω_c	0.24 ± 0.01
Baryonic matter	Ω_b	0.047 ± 0.002
Neutrinos	Ω_ν	< 0.02
Photons (CMB)	Ω_γ	5×10^{-5}
Total	Ω	1.003 ± 0.004
Curvature	Ω_k	-0.003 ± 0.004

10.12 Omega

Cosmologists designate the ratio of the actual density ρ of the Universe to the critical density ρ_crit by the fateful letter Ω, the final letter of the Greek alphabet,

$$\boxed{\Omega \equiv \frac{\rho}{\rho_\mathrm{crit}}} \,. \tag{10.46}$$

With no subscript, Ω denotes the total mass-energy density in all forms. A subscript x on Ω_x denotes mass-energy density of type x.

The curvature density ρ_k, which is not really a form of mass-energy but it is sometimes convenient to treat it as though it were, is defined by

$$\rho_k \equiv -\frac{3\kappa c^2}{8\pi G a^2} \,, \tag{10.47}$$

and correspondingly $\Omega_k \equiv \rho_k/\rho_\mathrm{crit}$. According to the first of Friedmann's equations (10.28), the curvature density Ω_k satisfies

$$\boxed{\Omega_k = 1 - \Omega} \,. \tag{10.48}$$

Note that Ω_k has opposite sign from κ, so a closed universe has negative Ω_k.

Table 10.1 gives measurements of Ω in various species, obtained by combining CMB data from WMAP, SPT, and ACT, Figure **??**, with supernova data, Figure 10.1, galaxy clustering (Baryonic Acoustic Oscillation, or BAO) data, Figure 10.3, and local measurements of the Hubble constant H_0 (Riess, Macri, et al., 2011). It is largely the CMB data that enable cosmological parameters to be measured to this level of precision. However, the CMB data are helped by the other data. Notably, the CMB data alone constrain the Hubble parameter relatively weakly, and the addition of BAO and direct measurements of H_0 help to resolve this uncertainty. Importantly, the various data are consistent with each other, inspiring confidence in the correctness of the Standard Model. The tightest error bars are obtained by combining all the data.

The cosmological parameters shift slightly if different prior theoretical assumptions are made. For example, a flat geometry, $\Omega = 1$, is consistent with observation, and is theoretically the most likely outcome of inflation.

If the geometry is constrained to be flat, then the value of the baryonic density tightens to $\Omega_{\rm b} = 0.046 \pm 0.001$, and the upper limit on neutrinos is reduced to $\Omega_\nu < 0.01$. The neutrino limit implies an upper limit to the sum of the masses of all neutrino species, which is, if the Universe is constrained to be flat,

$$\sum_\nu m_\nu < 0.4\,\mathrm{eV}\ . \tag{10.49}$$

Exercise 10.2 Omega in photons. Most of the energy density in electromagnetic radiation today is in CMB photons. Calculate Ω_γ in CMB photons. Note that photons may not be the only relativistic species today. Neutrinos with masses smaller than about $10^{-4}\,\mathrm{eV}$ would be still be relativistic at the present time, Exercise 10.19.

Solution. CMB photons have a blackbody spectrum at temperature $T_0 = 2.725\,\mathrm{K}$, so their density can be calculated from the blackbody formulae. The present day ratio Ω_γ of the mass-energy density ρ_γ of CMB photons to the critical density $\rho_{\rm crit}$ is

$$\Omega_\gamma \equiv \frac{\rho_\gamma}{\rho_{\rm crit}} = \frac{8\pi G \rho_\gamma}{3H_0^2} = \frac{8\pi^3 G (kT_0)^4}{45 H_0^2 c^5 \hbar^3} = 2.471 \times 10^{-5}\, h^{-2}\, T_{2.725\,\mathrm{K}}^4 = 5.2 \times 10^{-5}\, h_{0.69}^{-2}\, T_{2.725\,\mathrm{K}}^4\ . \tag{10.50}$$

10.13 Types of mass-energy

The energy-momentum tensor $T_{\mu\nu}$ of a FLRW Universe is necessarily homogeneous and isotropic, by assumption of the cosmological principle, taking the form (note yet again the trick of one index up and one down to remove the distorting effect of the metric)

$$T^\mu_{\ \nu} = \begin{pmatrix} T^t_t & 0 & 0 & 0 \\ 0 & T^r_r & 0 & 0 \\ 0 & 0 & T^\theta_\theta & 0 \\ 0 & 0 & 0 & T^\phi_\phi \end{pmatrix} = \begin{pmatrix} -\rho & 0 & 0 & 0 \\ 0 & p & 0 & 0 \\ 0 & 0 & p & 0 \\ 0 & 0 & 0 & p \end{pmatrix}\ . \tag{10.51}$$

Table 10.2 gives equations of state p/ρ for generic species of mass-energy, along with $(\rho + 3p)/\rho$, which determines the gravitational attraction (decleration) per unit energy, and how the mass-energy varies with cosmic scale factor, $\rho \propto a^n$, Exercise 10.3.

As commented in §10.9.2, the first law of thermodynamics for adiabatic expansion is built into Friedmann's equations. In fact the law represents covariant conservation of energy-momentum for the system as a whole

$$D_\mu T^{\mu\nu} = 0\ . \tag{10.52}$$

As long as species do not convert into each other (for example, no annihilation), covariant energy-momentum conservation holds individually for each species, so the first law applies to each species individually, determining how its energy density ρ varies with cosmic scale factor a. Figure 10.7 illustrates how the energy densities ρ of various species evolve as a function of scale factor a.

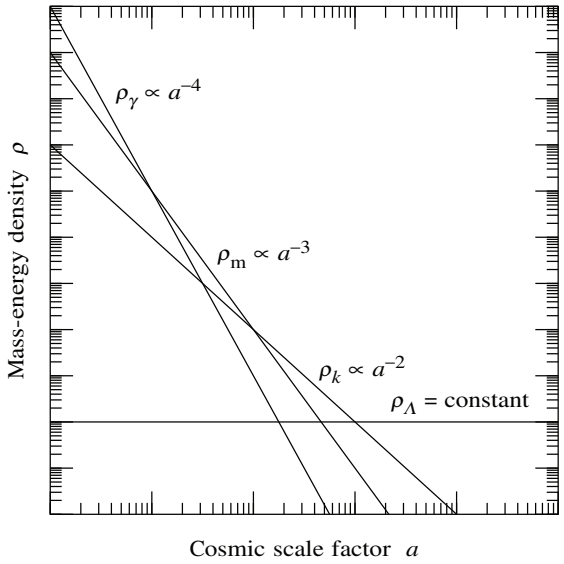

Figure 10.7 Behaviour of the mass-energy density ρ of various species as a function of cosmic time t.

Vacuum energy is equivalent to a **cosmological constant**. Einstein originally introduced the cosmological constant Λ as a modification to the left hand side of his equations,

$$G_{\kappa\mu} + \Lambda g_{\kappa\mu} = 8\pi G T_{\kappa\mu} \ . \tag{10.53}$$

The cosmological constant term can be taken over to the right hand side and reinterpreted as vacuum energy $T_{\kappa\mu} = -\rho_\Lambda \, g_{\kappa\mu}$ with energy density ρ_Λ, satisfying

$$\Lambda = 8\pi G \rho_\Lambda \ . \tag{10.54}$$

Table 10.2 *Properties of universes dominated by various species*

Species	p/ρ	$(\rho + 3p)/\rho$	$\rho \propto$
Radiation	1/3	2	a^{-4}
Matter	0	1	a^{-3}
Curvature	"−1/3"	"0"	a^{-2}
Vaccum	−1	−2	a^0

Exercise 10.3 Mass-energy in a FLRW Universe.

1. **First law.** The first law of thermodynamics for adiabatic expansion is built into Friedmann's equations (= Einstein's equations for the FLRW metric):

$$d(\rho a^3) + p\, da^3 = 0 \ . \tag{10.55}$$

   How does the density ρ evolve with cosmic scale factor for a species with equation of state $p/\rho = w$ with constant w. You should get an answer of the form

$$\rho \propto a^n \ . \tag{10.56}$$

2. **Attractive or repulsive?** For what equation of state w is the mass-energy attractive or repulsive? Consider in particular the cases of "matter," "radiation," and "vacuum" energy.

10.14 Redshifting

The spatial translation symmetry of the FLRW metric implies conservation of generalized momentum. As you will show in Exercise 10.4, a particle that moves along a geodesic in the radial direction, so that $d\theta = d\phi = 0$, has 4-velocity u^ν satisfying

$$u_{x_\parallel} = \text{constant} \ . \tag{10.57}$$

This conservation law implies that the proper momentum $p_{x_\parallel}$ of a radially moving particle decays as

$$p_{x_\parallel} \equiv ma\frac{dx_\parallel}{d\tau} \propto \frac{1}{a} \ , \tag{10.58}$$

which is true for both massive and massless particles.

It follows from equation (10.65) that light observed on Earth from a distant object will be redshifted by a factor

$$1 + z = \frac{a_0}{a} \ , \tag{10.59}$$

where a_0 is the present day cosmic scale factor. Cosmologists often refer to the redshift of an epoch, since the cosmological redshift is an observationally accessible quantity that uniquely determines the cosmic time of emission.

Exercise 10.4 Geodesics in the FLRW geometry. The Friedmann-Lemaître-Robertson-Walker metric of cosmology is

$$ds^2 = -\,dt^2 + a(t)^2\left[dx_\parallel^2 + \frac{\sin^2(\kappa^{1/2}x_\parallel)}{\kappa}\left(d\theta^2 + \sin^2\theta\, d\phi^2\right)\right] \ , \tag{10.60}$$

where κ is a constant, the curvature constant. Note that equation (10.60) is valid for all values of κ, including zero and negative values: there is no need to consider the cases separately.

1. **Conservation of generalized momentum.** Consider a particle moving along a geodesic in the radial direction, so that $d\theta = d\phi = 0$. Argue that the Lagrangian equations of motion

$$\frac{d}{d\tau}\frac{\partial L}{\partial u^{x_\parallel}} = \frac{\partial L}{\partial x_\parallel} \tag{10.61}$$

with effective Lagrangian

$$L = \tfrac{1}{2}\, g_{\mu\nu} u^\mu u^\nu \tag{10.62}$$

imply that

$$u_{x_\parallel} = \text{constant} \ . \tag{10.63}$$

Argue further from the same Lagrangian equations of motion that the assumption of a radial geodesic is valid because

$$u_\theta = u_\phi = 0 \tag{10.64}$$

is a consistent solution. [Hint: The metric $g_{\mu\nu}$ depends on the coordinate $x_\parallel$. But for radial geodesics with $u^\theta = u^\phi = 0$, the possible contributions from derivatives of the metric vanish.]

2. **Proper momentum.** Argue that a proper interval of distance measured by comoving observers along the radial geodesic is $a\, dx_\parallel$. Hence show from equation (10.63) that the proper momentum $p_{x_\parallel}$ of the particle relative to comoving observers (who are at rest in the FLRW metric) evolves as

$$p_{x_\parallel} \equiv ma\frac{dx_\parallel}{d\tau} \propto \frac{1}{a} \ . \tag{10.65}$$

3. **Redshift.** What relation does your result (10.65) imply between the redshift $1 + z$ of a distant object observed on Earth and the expansion factor a since the object emitted its light? [Hint: Equation (10.65) is valid for massless as well as massive particles. Why?]
4. **Temperature of the CMB.** Argue from the above results that the temperature T of the CMB evolves with cosmic scale factor as

$$T \propto \frac{1}{a} \ . \tag{10.66}$$

10.15 Evolution of the cosmic scale factor

Given how the energy density ρ of each species evolves with cosmic scale factor a, the first Friedmann equation then determines how the cosmic scale factor $a(t)$ itself evolves with cosmic time t. If the Hubble parameter $H \equiv \dot{a}/a$ is expressed as a function of cosmic scale factor a, then cosmic time t can be expressed in terms of a as

$$t = \int \frac{da}{aH} \ . \tag{10.67}$$

The definition (10.45) of the critical density allows the Hubble parameter H to be written

$$\frac{H}{H_0} = \sqrt{\frac{\rho_{\rm crit}}{\rho_{\rm crit}(a_0)}} \ . \tag{10.68}$$

The critical density $\rho_{\rm crit}$ is itself the sum of the densities ρ of all species *including* the curvature density,

$$\rho_{\rm crit} = \rho_k + \sum_{\text{species } x} \rho_x \ . \tag{10.69}$$

For example, in the case that the density is comprised of radiation, matter, and vacuum, the critical density is

$$\rho_{\rm crit} = \rho_{\rm r} + \rho_{\rm m} + \rho_k + \rho_\Lambda \ , \tag{10.70}$$

and equation (10.68) is

$$\frac{H(t)}{H_0} = \sqrt{\Omega_{\rm r} a^{-4} + \Omega_{\rm m} a^{-3} + \Omega_k a^{-2} + \Omega_\Lambda} \ , \tag{10.71}$$

where Ω_x represents its value at the present time. For density comprised of radiation, matter, and vacuum, equation (10.71), the time t, equation (10.67), is

$$t = \frac{1}{H_0} \int \frac{da}{a\sqrt{\Omega_{\rm r} a^{-4} + \Omega_{\rm m} a^{-3} + \Omega_k a^{-2} + \Omega_\Lambda}} \ , \tag{10.72}$$

which is an elliptic integral of the third kind. The elliptic integral simplifies to elementary functions in some cases relevant to reality, Exercises 10.5–10.7.

If one single species in particular dominates the mass-energy density, then equation (10.72) integrates to give the results in Table 10.3.

Table 10.3 *Evolution of cosmic scale factor in universes dominated by various species*

Dominant Species	$a \propto$
Radiation	$t^{1/2}$
Matter	$t^{2/3}$
Curvature	t
Vaccum	e^{Ht}

10.16 Age of the Universe

The present age t_0 of the Universe since the Big Bang can be derived from equation (10.72) and cosmological parameters, Table 10.1. Hinshaw et al. (2012) give the age of the Universe to be

$$t_0 = 13.7 \pm 0.2\,{\rm Gyr} \ . \tag{10.73}$$

The value tightens to $t_0 = 13.77 \pm 0.06\,\mathrm{Gyr}$ if the Universe is assumed to be flat.

Exercise 10.5 FLRW universe containing matter and vacuum. To a good approximation, the Universe today appears to be flat, and dominated by matter and a cosmological constant, with $\Omega_\mathrm{m} + \Omega_\Lambda = 1$. Show that in this case the relation between age t and cosmic scale factor a is

$$t = \frac{2}{3H_0\sqrt{\Omega_\Lambda}}\,\mathrm{asinh}\sqrt{\frac{\Omega_\Lambda a^3}{\Omega_\mathrm{m}}}\ . \tag{10.74}$$

Exercise 10.6 Age of the Universe. Evaluate the age t_0 of the Universe today ($a_0 = 1$) in the approximation that the Universe is flat and dominated by matter and a cosmological constant. [Note: Astronomers define one Julian year to be exactly 365.25 days of $24 \times 60 \times 60 = 86{,}400$ seconds each. A parsec (pc) is the distance at which a star has a parallax of 1 arcsecond, whence $1\,\mathrm{pc} = (60 \times 60 \times 180/\pi)\,\mathrm{au}$, where 1 au is one Astronomical Unit, the Earth-Sun distance. One Astronomical Unit was officially defined by the International Astronomical Union (IAU) in 2012 to be $1\,\mathrm{au} \equiv 149{,}597{,}870{,}700\,\mathrm{m}$, with official abbreviation au.]

Exercise 10.7 FLRW universe containing radiation plus matter. The Universe was dominated by radiation and matter over many decades of expansion including the time of recombination. Show that for a flat Universe containing radiation and matter the relation between age t and cosmic scale factor a is

$$t = \frac{2\Omega_\mathrm{r}^{3/2}}{3H_0\Omega_\mathrm{m}^2}\,\frac{\hat{a}^2(2+\sqrt{1+\hat{a}})}{(1+\sqrt{1+\hat{a}})^2}\ , \tag{10.75}$$

where $\hat{a}$ is the cosmic scale factor scaled to 1 at matter-radiation equality,

$$\hat{a} \equiv \frac{a}{a_\mathrm{eq}} = \frac{\Omega_\mathrm{m} a}{\Omega_\mathrm{r}}\ . \tag{10.76}$$

You may well find a formula different from (10.75), but you should be able to recover the latter using the identity $\sqrt{1+\hat{a}} - 1 = \hat{a}/(\sqrt{1+\hat{a}}+1)$. Equation (10.75) has the virtue that it is numerically stable to evaluate for all $\hat{a}$, including tiny $\hat{a}$.

10.17 Conformal time

It is often convenient to use **conformal time** η defined by (with units c temporarily restored)

$$a\,d\eta \equiv c\,dt\ , \tag{10.77}$$

with respect to which the FLRW metric is

$$\boxed{ds^2 = a(\eta)^2\left(-d\eta^2 + dx_\parallel^2 + x^2 do^2\right)}\ , \tag{10.78}$$

with x given by equation (10.19). The term conformal refers to a metric that is multiplied by an overall factor, the conformal factor (squared). In the FLRW metric (10.78), the cosmic scale factor a is the conformal factor.

Conformal time η is constructed so that radial null geodesics move at unit velocity in conformal coordinates. Light moving radially, with $d\theta = d\phi = 0$, towards an observer at the origin $x_\parallel = 0$ satisfies

$$\frac{dx_\parallel}{d\eta} = -1 \ . \tag{10.79}$$

10.18 Looking back along the lightcone

Since light moves radially at unit velocity in conformal coordinates, an object at geodesic distance $x_\parallel$ that emits light at conformal time $\eta_{\rm em}$ is observed at conformal time $\eta_{\rm obs}$ given by

$$\boxed{x_\parallel = \eta_{\rm obs} - \eta_{\rm em}} \ . \tag{10.80}$$

The comoving geodesic distance $x_\parallel$ to an object is

$$x_\parallel = \int_{\eta_{\rm em}}^{\eta_{\rm obs}} d\eta = \int_{t_{\rm em}}^{t_{\rm obs}} \frac{c\,dt}{a} = \int_{a_{\rm em}}^{a_{\rm obs}} \frac{c\,da}{a^2 H} = \int_0^z \frac{c\,dz}{H} \ , \tag{10.81}$$

where the last equation assumes the relation $1 + z = 1/a$, valid as long as a is normalized to unity at the observer (us) at the present time $a_{\rm obs} = a_0 = 1$. In the case that the density is comprised of (curvature and) radiation, matter, and vacuum, equation (10.81) gives

$$x_\parallel = \frac{c}{H_0} \int_{1/(1+z)}^1 \frac{da}{a^2 \sqrt{\Omega_{\rm r} a^{-4} + \Omega_{\rm m} a^{-3} + \Omega_k a^{-2} + \Omega_\Lambda}} \ , \tag{10.82}$$

which is an elliptical integral of the first kind. Given the geodesic comoving distance $x_\parallel$, the circumferential comoving distance x then follows as

$$x = \frac{\sinh(\sqrt{\Omega_k} H_0 x_\parallel / c)}{\sqrt{\Omega_k} H_0 / c} \ . \tag{10.83}$$

To second order in redshift z,

$$x \approx x_\parallel \approx \frac{c}{H_0} \left[z - z^2 \left(\Omega_{\rm r} + \tfrac{3}{4} \Omega_{\rm m} + \tfrac{1}{2} \Omega_{\rm k} \right) + ... \right] \ . \tag{10.84}$$

The geodesic and circumferential distances $x_\parallel$ and x differ at order z^3.

Figure 10.8 illustrates the relation between the comoving geodesic and circumferential distances $x_\parallel$ and x, equations (10.82) and (10.83), and redshift z, equation (10.59), in three cosmological models, including the standard flat ΛCDM model.

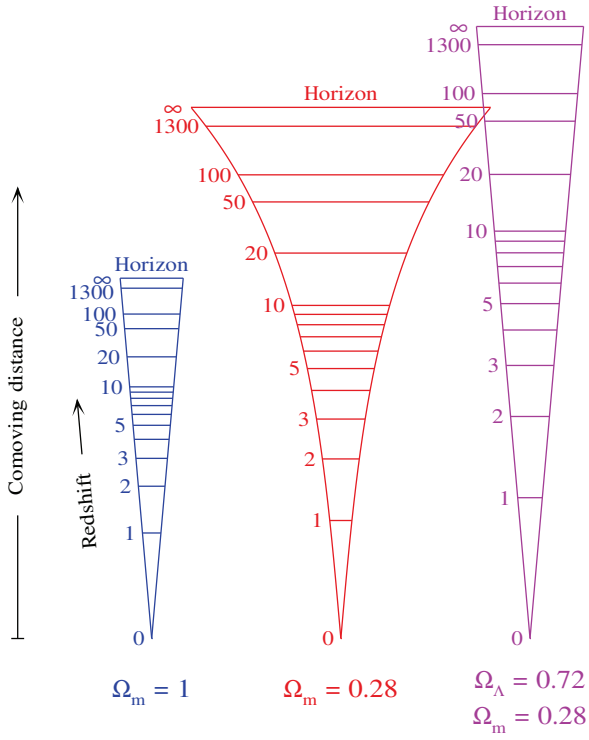

Figure 10.8 In this diagram, each wedge represents a cone of fixed opening angle, with the observer (us) at the point of the cone, at zero redshift. The wedges show the relation between physical sizes, namely the comoving distances $x_\parallel$ in the radial (vertical) and x in the transverse (horizontal) directions, and observable quantities, namely redshift and angular separation, in three different cosmological models: (left) a flat matter-dominated universe, (middle) an open matter-dominated universe, and (right) a flat ΛCDM universe.

10.19 Hubble diagram

The Hubble diagram of Type Ia supernova shown in Figure 10.1 is essentially a plot of (log) luminosity distance $\log d_L$ versus (log) redshift $\log z$. The luminosity distance is explained in §10.19.1 immediately following.

The vertical axis in the Hubble diagram 10.1 is actually in the astronomers' system of magnitudes. The magnitude system is described briefly in §10.19.2. Modulo an overall additive constant that equals the intrinsic absolute magnitude of a Type Ia standard candle, the apparent magnitude m of a supernova equals $5 \log d_L$, equation (10.89).

10.19.1 Luminosity distance

Astronomers conventionally define the **luminosity distance** d_L to a celestial object so that the observed flux F from the object (energy observed per unit time per unit collecting area of the telescope) is equal to the intrinsic luminosity L of the object (energy per unit time emitted by the object in its rest frame) divided by $4\pi d_L^2$,

$$F = \frac{L}{4\pi d_L^2} \ . \tag{10.85}$$

In other words, the luminosity distance d_L is defined so that flux F and luminosity L are related by the usual inverse square law of distance. Objects at cosmological distances are redshifted, so the luminosity at some emitted wavelength $\lambda_{\rm em}$ is observed at the redshifted wavelength $\lambda_{\rm obs} = \lambda_{\rm em}/(1+z)$. The luminosity distance (10.85) is defined so that the flux $F(\lambda_{\rm obs})$ on the left hand side is at the observed wavelength, while the luminosity $L(\lambda_{\rm em})$ on the right hand side is at the emitted wavelength. The observed flux and emitted luminosity are then related by

$$F = \frac{L}{(1+z)^2 4\pi x^2} \ , \tag{10.86}$$

where x is the comoving circumferential radius, normalized to $a_0 = 1$ at the present time. The factor of $1/(4\pi x^2)$ expresses the fact that the luminosity is spread over a sphere of proper area $4\pi x^2$. Equation (10.86) involves two factors of $1+z$, one of which come from the fact that the observed photon energy is redshifted, and the other from the fact that the observed number of photons detected per unit time is redshifted by $1+z$. Equations (10.85) and (10.86) imply the luminosity distance d_L is related to the circumferential distance x and the redshift z by

$$d_L = (1+z)x \ . \tag{10.87}$$

Why bother with the luminosity distance if it can be reduced to the circumferential distance x by dividing by a redshift factor? The answer is that, especially historically, fluxes of distant astronomical objects are often measured from images without direct spectral information. If the intrinsic luminosity of the object is treated as "known" (as with Cepheid variables and Type Ia supernovae), then the luminosity distance $d_L = \sqrt{L/(4\pi F)}$ can be inferred without knowledge of the redshift. In practice objects are often measured with a fixed colour filter or set of filters, and some additional correction, historically called the K-correction, is necessary to transform the flux in an observed filter to a common band.

10.19.2 Magnitudes

The Hubble diagram of Type Ia supernova shown in Figure 10.1 has for its vertical axis the astronomers' system of magnitudes, a system that dates back to the 2nd century BC Greek astronomer Hipparchus.

A magnitude is a logarithmic measure of brightness, defined such that an interval of 5 magnitudes m corresponds to a factor of 100 in linear flux F. Following Hipparchus, the magnitude system is devised such that the brightest stars in the sky have apparent magnitudes of approximately 0, while fainter stars have

larger magnitudes, the faintest naked eye stars in the sky being about magnitude 6. Traditionally, the system is tied to the star Vega, which is defined to have magnitude 0. Thus the apparent magnitude m of a star is

$$m = m_{\rm Vega} - 2.5 \log \left(F / F_{\rm Vega} \right) \ . \tag{10.88}$$

The absolute magnitude M of an object is defined to equal the apparent magnitude m that it would have if it were 10 parsecs away, which is the approximate distance to the star Vega. Thus

$$m - M = 5 \log \left(d_L / 10 \, {\rm pc} \right) \ , \tag{10.89}$$

where d_L is the luminosity distance.

Exercise 10.8 Hubble diagram. Draw a theoretical Hubble diagram, a plot of luminosity distance d_L versus redshift z, for universes with various values of Ω_Λ and $\Omega_{\rm m}$. The relation between d_L and z is an elliptic integral of the first kind, so you will need to find a program that does elliptic integrals (alternatively, you can do the integral numerically). The elliptic integral simplifies to elementary functions in simple cases where the mass-energy density is dominated by a single component (either mass $\Omega_{\rm m} = 1$, or curvature $\Omega_{\rm k} = 1$, or a cosmological constant $\Omega_\Lambda = 1$).
Solution. Your model curves should look similar to those in Figure 10.1.

10.20 Recombination

The CMB comes to us from the epoch of **recombination**, when the Universe transitioned from being mostly ionized, and therefore opaque, to mostly neutral, and therefore transparent. As the Universe expands, the temperature of the cosmic background decreases as $T \propto a^{-1}$. Given that the CMB temperature today is $T_0 \approx 3 \, {\rm K}$, the temperature would have been about 3,000K at a redshift of about 1,000. This temperature corresponds to the temperature at which hydrogen, the most abundant element in the Universe, ionizes. Not coincidentally, the temperature of recombination is comparable to the $\approx 5{,}800 \, {\rm K}$ surface temperature of the Sun. The CMB and Sun temperatures differ because the baryon-to-photon number density is much greater in the Sun.

The transition from mostly ionized to mostly neutral takes place over a fairly narrow range of redshifts, just as the transition from ionized to neutral at the photosphere of the Sun is rather sharp. Thus recombination can be approximated as occurring almost instantaneously. Hinshaw et al. (2012, supplementary data) distinguish the redshift $z_{\rm rec}$ of recombination, when the number of ionized and neutral atoms were equal, and the redshift z_* at which the photon-electron scattering (Thomson) optical depth was 1,

$$z_{\rm rec} = 1089 \pm 1 \ , \quad z_* = 1092 \pm 1 \ . \tag{10.90}$$

The age of the Universe at recombination was

$$t_* = 376{,}000 \pm 4{,}000 \, {\rm yr} \ . \tag{10.91}$$

10.21 Horizon

Light can come from no more distant point than the Big Bang. This distant point defines what cosmologists traditionally refer to as the **horizon** (or particle horizon) of our Universe, located at infinite redshift, $z = \infty$. Equation (10.81) gives the geodesic distance between us at redshift zero and the horizon as

$$x_\parallel(\text{horizon}) = \int_0^\infty \frac{c\,dz}{H} \ . \tag{10.92}$$

The standard ΛCDM paradigm is based in part on the proposition that the Universe had an early inflationary phase, §10.22. If so, then there is no place where the redshift reaches infinity. However, the redshift

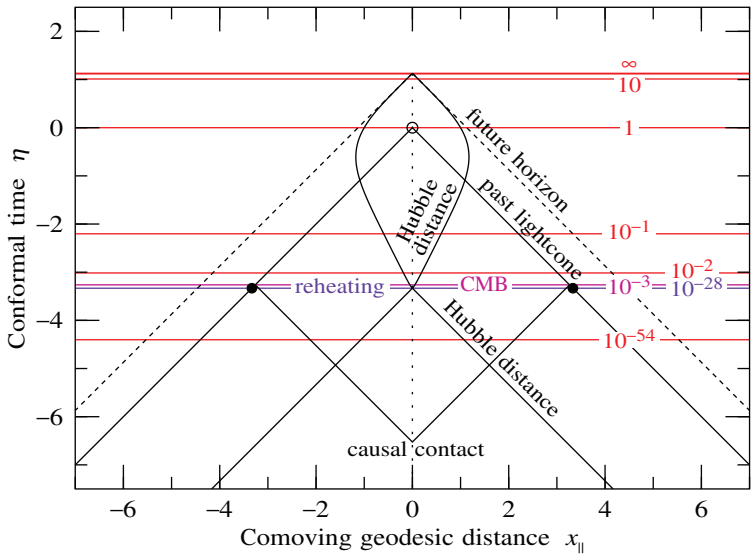

Figure 10.9 Spacetime diagram of a FLRW Universe in conformal coordinates η and $x_\parallel$, in units of the present day Hubble distance c/H_0. The unfilled circle marks our position, which is taken to be the origin of the conformal coordinates. In conformal coordinates, light moves at 45° on the spacetime diagram. The diagram is drawn for a flat ΛCDM model with $\Omega_\Lambda = 0.72$, $\Omega_\mathrm{m} = 0.28$, and a radiation density such that the redshift of matter-radiation equality is 3200, consistent with Hinshaw et al. (2012). Horizontal lines are lines of constant cosmic scale factor a, labelled by their values relative to the present, $a_0 = 1$. Reheating, at the end of inflation, has been taken to be at redshift 10^{28}. Filled dots mark the place that cosmologists traditionally call the horizon, at reheating, which is a place of large, but not infinite, redshift. Inflation offers a solution to the horizon problem because all points on the CMB within our past lightcone could have been in causal contact at an early stage of inflation. If dark energy behaves like a cosmological constant into the indefinite future, then we will have a future horizon.

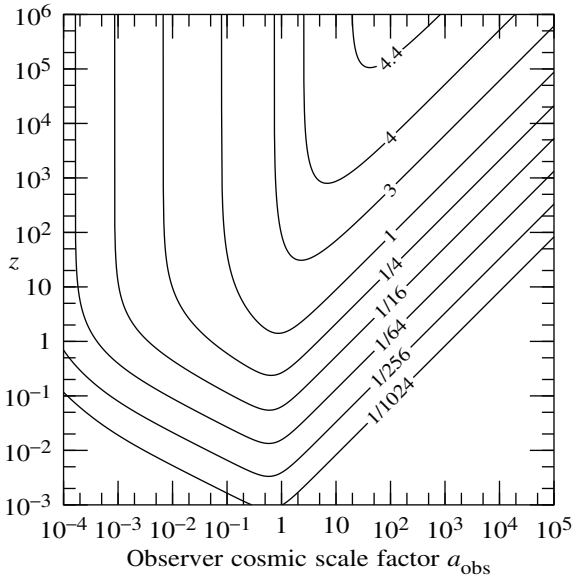

Figure 10.10 Redshift z of objects at fixed comoving distances as a function of the epoch $a_{\rm obs}$ at which an observer observes them. The label on each line is the comoving distance $x_\parallel$ in units of c/H_0. The diagram is drawn for a flat ΛCDM model with $\Omega_\Lambda = 0.72$, $\Omega_{\rm m} = 0.28$, and a radiation density such that the redshift of matter-radiation equality is 3200. The present-day Universe, at $a_{\rm obs} = 1$, is transitioning from a decelerating, matter-dominated phase to an accelerating, vacuum-dominated phase. Whereas in the past redshifts tended to decrease with time, in the future redshifts will tend to increase with time.

is large at reheating, when inflation ends, and cosmologists call this the horizon,

$$x_\parallel(\text{horizon}) = \int_0^{\text{huge}} \frac{c\,dz}{H} \ . \tag{10.93}$$

Figure 10.9 shows a spacetime diagram of a FLRW Universe with cosmological parameters consistent with those of Hinshaw et al. (2012). In this model, the comoving horizon distance to reheating is

$$x_\parallel(\text{horizon}) = 3.333\,c/H_0 = 14.5\,\text{Gpc} = 4.72\,\text{Glyr} \ . \tag{10.94}$$

The redshift of reheating in this model has been taken at $z = 10^{28}$, but the horizon distance is insensitive to the choice of reheating redshift.

The horizon should be distinguished from the future horizon, which Hawking and Ellis (1973) define to be the farthest that an observer will ever be able to see in the indefinite future. If the Universe continues accelerating, as it is currently, then our future horizon will be finite, as illustrated in Figure 10.9.

A quantity that cosmologists sometimes refer to loosely as the horizon is the **Hubble distance**, defined

to be

$$\text{Hubble distance} \equiv \frac{c}{H} \ , \tag{10.95}$$

The Hubble distance sets the characteristic scale over which two observers can communicate and influence each other, which is smaller than the horizon distance.

The standard ΛCDM model has the curious property that the Universe is switching from a matter-dominated period of deceleration to a vacuum-dominated period of acceleration. During deceleration, objects appear over the horizon, while during acceleration, they disappear over the horizon. Figure 10.10 illustrates the evolution of the observed redshifts of objects at fixed comoving distances. In the past decelerating phase, the redshift of objects appearing over the horizon decreased rapidly from some huge value. In the future accelerating phase, the redshift of objects disappearing over the horizon will increase in proportion to the cosmic scale factor.

10.22 Inflation

Part of the Standard Model of Cosmology is the hypothesis that the early Universe underwent a period of **inflation**, when the mass-energy density was dominated by "vacuum" energy, and the Universe expanded exponentially, with $a \propto e^{Ht}$. The idea of inflation was originally motivated around 1980 by the idea that early in the Universe the forces of nature would be unified, and that there is energy associated with that unification. For example, the inflationary energy could be the energy associated with Grand Unification of the $U(1) \times SU(2) \times SU(3)$ forces of the standard model. The three coupling constants of the standard model vary slowly with energy, appearing to converge at an energy of around $m_{\rm GUT} \sim 10^{16}\,{\rm GeV}$, not much less than the Planck energy of $m_{\rm P} \sim 10^{19}\,{\rm GeV}$. The associated vacuum energy density would be of order $\rho_{\rm GUT} \sim m_{\rm GUT}^4$ in Planck units.

Alan Guth (1981) pointed at that, regardless of theoretical arguments for inflation, an early inflationary epoch would solve a number of observational conundra. The most important observational problem is the **horizon problem**, Exercise 10.10. If the Universe has always been dominated by radiation and matter, and therefore always decelerating, then up to the time of recombination light could only have travelled a distance corresponding to about 1 degree on the cosmic microwave background sky, Exercise 10.9. If that were the case, then how come the temperature at points in the cosmic microwave background more than a degree apart, indeed even 180° apart, on opposite sides of the sky, have the same temperature, even though they could never have been in causal contact? Guth pointed out that inflation could solve the horizon problem by allowing points to be initially in causal contact, then driven out of causal contact by the acceleration and consequent exponential expansion induced by vacuum energy, provide that the inflationary expansion continued over a sufficient number e-folds, Exercise 10.10. Guth's solution is illustrated in the spacetime diagram in Figure 10.9.

Guth pointed out that inflation could solve some other problems, such as the **flatness problem**. However, most of these problems are essentially equivalent to the horizon problem, Exercise 10.11.

A basic problem that inflation solves is the **expansion problem**. If the Universe has always been dominated by a gravitationally attractive form of mass-energy, such as matter or radiation, then how come the Universe is expanding? Inflation solves the problem because an initial period dominated by gravitationally repulsive vacuum energy could have accelerated the Universe into enormous expansion.

Inflation also offers an answer to the question of where the matter and radiation seen in the Universe today came from. Inflation must have come to an end, since the present day Universe does not contain the enormously high vacuum energy density that dominated during inflation (the vacuum energy during inflation was vast compared to the present-day cosmological constant). The vacuum energy must therefore have decayed into other forms of gravitationally attractive energy, such as matter and radiation. The process of decay is called **reheating**. Reheating is not well understood, because it occurred at energies well above those accessible to experiment today. Nevertheless, if inflation occurred, then so also did reheating.

Compelling evidence in favour of the inflationary paradigm comes from the fact that, in its simplest form, inflationary predictions for the power spectrum of fluctuations of the CMB fit astonishingly well to observational data, which continue to grow ever more precise.

Exercise 10.9 Horizon size at recombination.

1. **Comoving horizon distance.** Assume for simplicity a flat, matter-dominated Universe. From equation (10.92), what is the comoving horizon distance $x_{\parallel}$ as a function of cosmic scale factor a?
2. **Angular size on the CMB of the horizon at recombination.** For a flat Universe, the angular size on the CMB of the horizon at recombination equals the ratio of the comoving horizon distance at recombination to the comoving distance between us and recombination. Recombination occurs at sufficiently high redshift that the latter distance approximates the comoving horizon at the present time. Estimate the angular size on the CMB of the horizon at recombination if the redshift of recombination is $z_{\rm rec} \approx 1000$.

Exercise 10.10 The horizon problem.

1. **Expansion factor.** The temperature of the CMB today is $T_0 \approx 3\,\mathrm{K}$. By approximately what factor has the Universe expanded since the temperature was some initial high temperature, say the GUT temperature $T_{\rm i} \approx 10^{29}\,\mathrm{K}$, or the Planck temperature $T_{\rm i} \approx 10^{32}\,\mathrm{K}$?
2. **Hubble distance.** By what factor has the Hubble distance c/H increased during the expansion of part 1.? Assume for simplicity that the Universe has been mainly radiation-dominated during this period, and that the Universe is flat. [Hint: For a flat Universe $H^2 \propto \rho$, and for radiation-dominated Universe $\rho \propto a^{-4}$.]
3. **Comoving Hubble distance.** Hence determine by what factor the comoving Hubble distance $x_H = c/(aH)$ has increased during the expansion of part 1..
4. **Comoving Hubble distance during inflation.** During inflation the Hubble distance c/H remained constant, while the cosmic scale factor a expanded exponentially. What is the relation between the comoving Hubble distance $x_H = c/(aH)$ and cosmic scale factor a during inflation? [You should obtain an answer of the form $x_H \propto a^{?}$.]

5. **Number of e-foldings to solve the horizon problem.** By how many e-foldings must the Universe have inflated in order to solve the horizon problem? Assume again, as in part 1., that the Universe has been mainly radiation-dominated during expansion from the Planck temperature to the current temperature, and that this radiation-dominated epoch was immediately preceded by a period of inflation. [Hint: Inflation solves the horizon problem if the currently observable Universe was within the Hubble distance at the beginning of inflation, i.e. if the comoving $x_{H,0}$ now is less than the comoving Hubble distance $x_{H,i}$ at the beginning of inflation. The 'number of e-foldings' is $\ln(a_\mathrm{f}/a_\mathrm{i})$, where ln is the natural logarithm, and a_i and a_f are the cosmic scale factors at the beginning (i for initial) and end (f for final) of inflation.]

Exercise 10.11 Relation between horizon and flatness problems. Show that Friedmann's equation (10.28a) can be written in the form

$$\Omega - 1 = \kappa x_H^2 \ , \tag{10.96}$$

where $x_H \equiv c/(aH)$ is the comoving Hubble distance. Use this equation to argue in your own words how the horizon and flatness problems are related.

10.23 Evolution of the size and density of the Universe

Figure 10.11 shows the evolution of the cosmic scale factor a as a function of time t predicted by the standard flat ΛCDM model, coupled with a plausible depiction of the early inflationary epoch. The parameters of the model are the same as those for Figure 10.9. In the model, the Universe starts with an inflationary phase, and transitions instantaneously at reheating to a radiation-dominated phases. Not long before recombination, the Universe goes over to a matter-dominated phase, then later to the dark-energy-dominated phase of today. The relation between cosmic time t and cosmic scale factor a is given by equation (10.67), and some relevant analytic results are in Exercises 10.5 and 10.7.

Figure 10.11 also shows the evolution of the Hubble distance c/H, which sets the approximate scale within which regions are in causal contact. The Hubble distance is constant during vacuum-dominated phases, but is approximately proportional to the age of the Universe at other times. The Figure illustrates that regions that are in causal contact prior to inflation can fly out of causal contact during the accelerated expansion of inflation. Once the Universe transitions to a decelerating radiation- or matter-dominated phase, regions that were out of causal contact can come back into causal contact, inside the Hubble distance.

Since inflation occurred at high energies inaccessible to experiment, the energy scale of inflation is unknown, and the number of e-folds during which inflation persisted is unknown. Figure 10.11 illustrates the case where the energy scale of inflation is around the GUT scale, and the number of e-folds is only slightly greater than the number necessary to solve the horizon problem. Figure 10.11 does not attempt to extrapolate to what might possibly have happened prior to inflation, a problem that is the topic of much speculation by theoretical physicists.

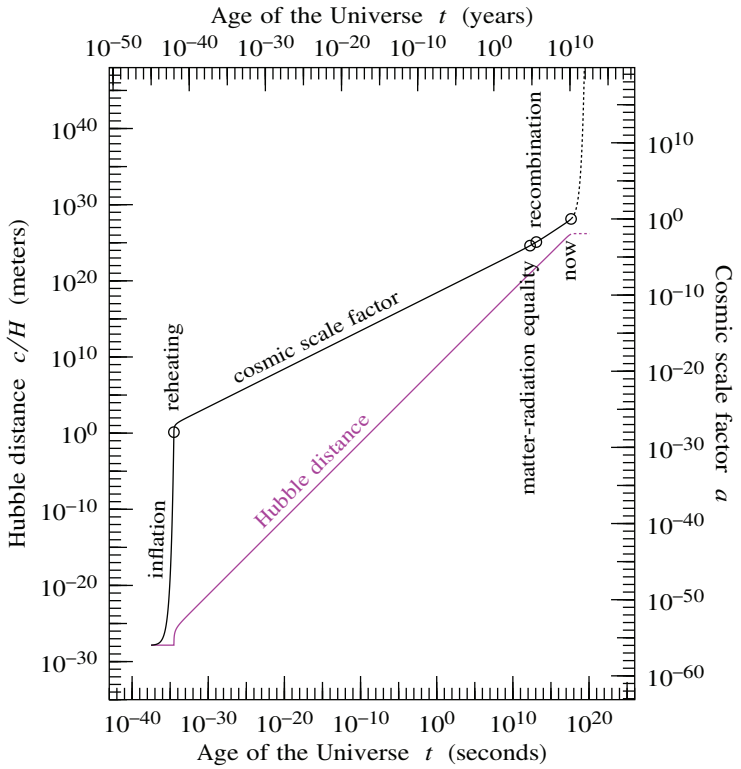

Figure 10.11 Cosmic scale factor a and Hubble distance c/H as a function of cosmic time t, for a flat ΛCDM model with the same parameters as in Figure 10.9. In this model, the Universe began with an inflationary epoch where the density was dominated by constant vacuum energy, the Hubble parameter H was constant, and the cosmic scale factor increased exponentially, $a \propto e^{Ht}$. The initial inflationary phase came to an end when the vacuum energy decayed into radiation energy, an event called reheating. The Universe then became radiation-dominated, evolving as $a \propto t^{1/2}$. At a redshift of $z_{\rm eq} \approx 3200$ the Universe passed through the epoch of matter-radiation equality, where the density of radiation equalled that of (non-baryonic plus baryonic) matter. Matter-radiation equality occurred just prior to recombination, at $z_{\rm rec} \approx 1090$. The Universe remained matter-dominated, evolving as $a \propto t^{2/3}$, until relatively recently (from a cosmological perspective). The Universe transitioned through matter-dark energy equality at $z_\Lambda \approx 0.4$. The dotted line shows how the cosmic scale factor and Hubble distance will evolve in the future, if the dark energy is a cosmological constant, and if it does not decay into some other form of energy.

Figure 10.12 shows the mass-energy density ρ as a function of time t for the same flat ΛCDM model as shown in Figure 10.11. Since the Universe here is taken to be flat, the density equals the critical density at all times, and is proportional to the inverse square of the Hubble distance c/H plotted in Figure 10.11.

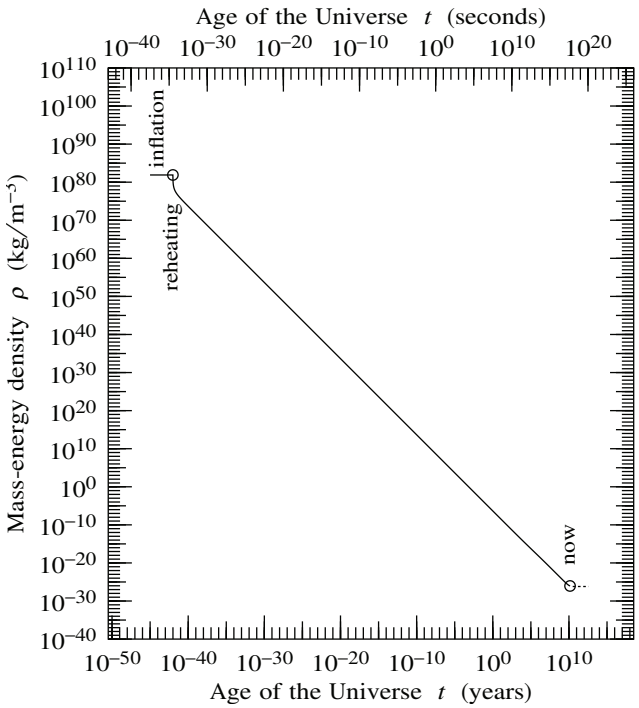

Figure 10.12 Mass-energy density ρ of the Universe as a function of cosmic time t corresponding to the evolution of the cosmic scale factor shown in Figure 10.11.

The energy density is constant during epochs dominated by vacuum energy, but decreases approximately as $\rho \propto t^{-2}$ at other times.

10.24 Evolution of the temperature of the Universe

A system of photons in thermodynamic equilibrium has a blackbody distribution of energies. The CMB has a precise blackbody spectrum, not because it is in thermodynamic equilibrium today, but rather because the CMB was in thermodynamic equilibrium with electrons and nuclei at the time of recombination, and the CMB has streamed more or less freely through the Universe since recombination. A thermal distribution of relativistic particles retains its thermal distribution in an expanding FLRW universe (albeit with a changing temperature), Exercise 10.12.

The evolution of the temperature of photons in the Universe can be deduced from conservation of entropy. The Friedmann equations imply the first law of thermodynamics, §10.9.2, and thus enforce conservation

of entropy per comoving volume. Entropy is conserved in a FLRW universe even when particles annihilate with each other. For example, electrons and positrons annihilated with each other when the temperature fell through $T \approx m_e = 511\,\mathrm{keV}$, but the entropy lost by electrons and positrons was gained by photons, for no net change in entropy, Exercise 10.13.

In the real Universe, entropy increases as a result of fluctuations away from the perfect homogeneity and isotropy assumed by the FLRW geometry. By far the biggest repositories of entropy in today's Universe are black holes, principally supermassive black holes. However, black holes are essentially irrelevant to the CMB. It is fine to compute the temperature of cosmological radiation from conservation of cosmological entropy.

The entropy of a system in thermodynamic equilibrium is approximately one per particle, Exercise 10.17. The number of particles in the Universe today is dominated by particles that were relativistic at the time they decoupled, namely photons and neutrinos, and these therefore dominate the cosmological entropy. The ratio $\eta_b \equiv n_b/n_\gamma$ of baryon to photon number in the Universe today is less than a billionth,

$$\eta_b \equiv \frac{n_b}{n_\gamma} = \frac{\epsilon_\gamma \Omega_b}{m_b \Omega_\gamma} = 2.73 \times 10^{-8}\, \Omega_b h^2 T_{2.725\,\mathrm{K}}^{-3} = 6.0 \times 10^{-10}\ , \tag{10.97}$$

where $\epsilon_\gamma = \pi^4 T_0/(30\zeta(3)) = 2.701\, T_0$ is the mean energy per photon (Exercise 10.14), and $m_b = 939\,\mathrm{MeV}$ is the approximate mass per baryon.

Conservation of entropy per comoving volume implies that the photon temperature T at redshift z is related to the present day photon temperature T_0 by (Exercise 10.18)

$$\frac{T}{T_0} = (1+z)\left(\frac{g_{s,0}}{g_s}\right)^{1/3}\ , \tag{10.98}$$

where g_s is the entropy-weighted effective number of relativistic particle species.

The other major contributors to cosmological entropy today, besides photons, are neutrinos and antineutrinos. Neutrinos decoupled at a temperature of about $T \approx 1\,\mathrm{MeV}$. Above that temperature weak interactions were fast enough to keep neutrinos and antineutrinos in thermodynamic equilibrium with protons and neutrons, hence with photons, but below that temperature neutrinos and antineutrinos froze out. It is expected that there should be a Cosmic Neutrino Background (CNB) analogous to the CMB. Sadly, neutrinos interact too weakly for such a background to be detectable with current technology. Like the CMB, the CNB should have a (redshifted) thermal distribution inherited from being in thermodynamic equilibrium at $T \sim 1\,\mathrm{MeV}$.

Because neutrinos froze out before $e\bar{e}$-annihilation, annihilating electrons and positrons dumped their entropy into photons, increasing the temperature of photons relative to that of neutrinos. The temperature of the CNB today is, Exercise 10.19,

$$T_\nu = \left(\frac{4}{11}\right)^{1/3} 2.725\,\mathrm{K} = 1.945\,\mathrm{K}\ . \tag{10.99}$$

Table 10.4 gives approximate values of the effective entropy-weighted number g_s of relativistic particle species over various temperature ranges. The extra factor of two for g_s in the final column of Table 10.4 arises because every particle species has an antiparticle (the two spin states of a photon can be construed as each other's antiparticle). The entropy of a relativistic fermionic species is 7/8 that of a bosonic species,

Exercise 10.15, equation (10.127). The difference in photon and neutrino temperatures leads to an extra factor of 4/11 in the value of g_s today, which, with 1 bosonic species (photons) and 3 fermionic species (neutrinos), together with their antiparticles, is, equation (10.138),

$$g_{s,0} = 2\left(1 + \frac{7}{8}\frac{4}{11}3\right) = \frac{43}{11} = 3.91\ . \tag{10.100}$$

A more comprehensive evaluation of g_s is given by Kolb and Turner (1990, Fig. 3.5). Over the range of energies $T \lesssim 1\,\mathrm{TeV}$ covered by the standard model of physics, there are four principal epochs in the evolution of the effective number g_s of relativistic species, punctuated by electron-positron annihilation at $T \approx 0.5\,\mathrm{MeV}$, the QCD phase transition from bound nuclei to free quarks and gluons at $T \approx 100\,\mathrm{MeV}$, and the electroweak phase transition above which all standard model particles are relativistic at $T \approx 100\,\mathrm{GeV}$. There could well be further changes in the number of relativistic species at higher temperatures, for example if supersymmetry becomes unbroken at some energy, but at present no experimental data constrain the possibilities.

Table 10.4 *Effective entropy-weighted number of relativistic particle species*

Temperature T	particles	spin	chiralities	generations	flavours	colours	multiplicity	g_s
$T \lesssim 0.5\,\mathrm{MeV}$	photon γ	1					1	$2\left(1 + \frac{7}{8}\frac{4}{11}3\right) = 3.91$
	neutrinos ν_e, ν_μ, ν_τ	$\frac{1}{2}$	1	3			3	
$0.5\,\mathrm{MeV} \lesssim T \lesssim 100\,\mathrm{MeV}$	photon γ	1					1	$2\left(1 + \frac{7}{8}5\right) = 10.75$
	neutrinos ν_e, ν_μ, ν_τ	$\frac{1}{2}$	1	3			3	
	electron e	$\frac{1}{2}$	2	1			2	
$100\,\mathrm{MeV} \lesssim T \lesssim 100\,\mathrm{GeV}$	photon γ	1					1	$2\left(9 + \frac{7}{8}33\right) = 75.75$
	$SU(3)$ gluons	1					8	
	neutrinos ν_e, ν_μ, ν_τ	$\frac{1}{2}$	1	3			3	
	leptons e, μ	$\frac{1}{2}$	2	2			6	
	quarks u, d, c, s	$\frac{1}{2}$	2	2	2	3	24	
$T \gtrsim 100\,\mathrm{GeV}$	$SU(2) \times U_Y(1)$ gauge bosons	1					$3 + 1$	$2\left(14 + \frac{7}{8}45\right) = 106.75$
	$SU(3)$ gluons	1					8	
	complex Higgs	0					2	
	neutrinos ν_e, ν_μ, ν_τ	$\frac{1}{2}$	1	3			3	
	leptons e, μ, τ	$\frac{1}{2}$	2	3			6	
	quarks u, d, c, s, t, b	$\frac{1}{2}$	2	3	2	3	36	

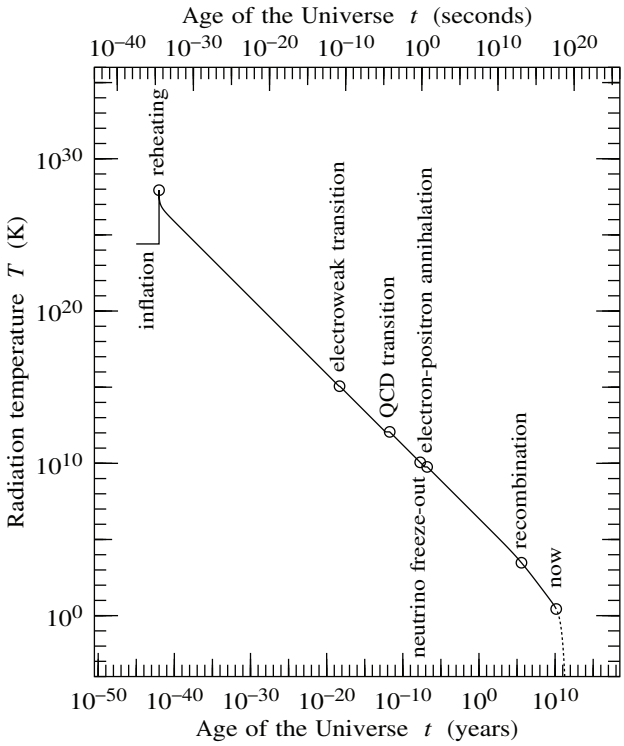

Figure 10.13 Radiation temperature T of the Universe as a function of cosmic time t corresponding to the evolution of the cosmic scale factor shown in Figure 10.11. The temperature during inflation was the Hawking temperature, equal to $H/(2\pi)$ in Planck units. After inflation and reheating, the temperature decreases as $T \propto a^{-1}$, modified by a factor depending on the effective entropy-weighted number g_s of particle species, equation (10.98). In this plot, the effective number g_s of relativistic particle species has been approximated as changing at three discrete points, electron-positron annihilation, the QCD phase transition, and the electroweak phase transition, Table 10.4.

Figure 10.13 shows the radiation (photon) temperature T as a function of time t corresponding to the evolution of the scale factor a and temperature T shown in Figures 10.11 and 10.12.

10.25 Neutrino mass

Neutrinos are created naturally by nucleosynthesis in the Sun, and by interaction of cosmic rays with the atmosphere. When a neutrino is created (or annihilated) by a weak interaction, it is created in a weak eigenstate. Observations of solar and atmospheric neutrinos indicate that neutrino species oscillate into each

other, implying that the weak eigenstates are not mass eigenstates. The weak eigenstates are denoted ν_e, ν_μ, and ν_τ, while the mass eigenstates are denoted ν_1, ν_2, and ν_3. Oscillation data yield mass squared differences between the three mass eigenstates (Forero, Tortola, and Valle, 2012)

$$|\Delta m_{21}|^2 = 7.6 \pm 0.2 \times 10^{-5}\,\mathrm{eV}^2 \quad \text{solar neutrinos}\ , \tag{10.101a}$$

$$|\Delta m_{31}|^2 = 2.4 \pm 0.1 \times 10^{-3}\,\mathrm{eV}^2 \quad \text{atmospheric neutrinos}\ . \tag{10.101b}$$

The data imply that at least two of the neutrino types have mass. The squared mass difference between m_1 and m_2 implies that at least one of them must have a mass

$$m_{\nu_1} \text{ or } m_{\nu_2} \geq \sqrt{7.6 \times 10^{-5}\,\mathrm{eV}^2} \approx 0.01\,\mathrm{eV}\ . \tag{10.102}$$

The squared mass difference between m_1 and m_3 implies that at least one of them must have a mass

$$m_{\nu_1} \text{ or } m_{\nu_3} \geq \sqrt{2.4 \times 10^{-3}\,\mathrm{eV}^2} \approx 0.05\,\mathrm{eV}\ . \tag{10.103}$$

The ordering of masses is undetermined by the data. The natural ordering is $m_1 < m_2 < m_3$, but an inverted hierarchy $m_3 < m_1 \approx m_2$ is possible.

The CNB temperature, equation (10.99), is $T_\nu = 1.945\,\mathrm{K} = 1.676 \times 10^{-4}\,\mathrm{eV}$. The redshift at which a neutrino of mass m_ν becomes non-relativistic is then

$$1 + z_\nu = \frac{m_\nu}{T_\nu} = \frac{m_\nu}{1.676 \times 10^{-4}\,\mathrm{eV}}\ . \tag{10.104}$$

Neutrinos of masses 0.01 eV and 0.05 eV would have become non-relativistic at $z_\nu \approx 60$ and 300 respectively. Only a neutrino of mass $\lesssim 10^{-4}$ eV would remain relativistic at the present time.

The masses from neutrino oscillation data suggest that at least two species of cosmological neutrinos are non-relativistic today. If so, then the neutrino density Ω_ν today is related to the sum $\sum m_\nu$ of neutrino masses by

$$\Omega_\nu = \frac{8\pi G \sum m_\nu n_\nu}{3H_0^2} = 5.6 \times 10^{-4} \left(\frac{\sum m_\nu}{0.05\,\mathrm{eV}} \right) h_{0.69}^{-2}\ . \tag{10.105}$$

The number and entropy densities of neutrinos today are unaffected by whether they are relativistic, so the effective number- and entropy-weighted numbers $g_{n,0}$ and $g_{s,0}$ are unaffected. On the other hand the energy density of neutrinos today does depend on whether or not they are relativistic. If just one neutrino type is relativistic and the other two are non-relativistic, then the effective energy-weighted number $g_{\rho,0}$ of relativistic species today is

$$g_{\rho,0} = 2 + \left(\frac{4}{11} \right)^{4/3} \frac{7}{8}\, 2 = 2.45\ . \tag{10.106}$$

The density Ω_r of relativistic particles today is $\Omega_\mathrm{r} = (g_{\rho,0}/2)\Omega_\gamma$.

10.26 Occupation number, number density, and energy-momentum

A careful treatment of the evolution of the number and energy-momentum densities of species in a FLRW universe requires consideration of their momentum distributions.

10.26.1 Occupation number

Choose a locally inertial frame attached to an observer. The distribution of a particle species (distinct spin states being regarded as distinct species) in the observer's frame is described by a scalar occupation number $f(x^\mu, \boldsymbol{p})$ that specifies the number dN of particles at the observer's position x^μ with momentum $p^k \equiv \{E, \boldsymbol{p}\}$ in a Lorentz-invariant 6-dimensional volume of phase space,

$$dN = f(x^\mu, \boldsymbol{p})\, \frac{d^3r\, d^3p}{(2\pi\hbar)^3}\ . \tag{10.107}$$

Here d^3r and d^3p denote the proper spatial and momentum 3-volume elements in the observer's frame.

The phase volume element $d^3r\, d^3p$ is a scalar, invariant under Lorentz transformations of the observer's frame. This can be proved as follows. First, the 3-volume element d^3r is related to the scalar 4-volume element $dt\, d^3r$ by[1]

$$\frac{dt\, d^3r}{d\lambda} = E\, d^3r\ , \tag{10.108}$$

since $dt/d\lambda = E$. The left hand side of equation (10.108) is the derivative of the observer's 4-volume $dt\, d^3r$ with respect to the observer's affine parameter $d\lambda \equiv d\tau/m_{\rm obs}$. Since both of these are scalars, it follows that $E\, d^3r$ is a scalar. Second, the momentum 3-volume element d^3p is related to the scalar 4-volume element $dE\, d^3p$ by

$$\delta(E^2 - p^2 - m^2)\, dE\, d^3p = \frac{d^3p}{2E}\ , \tag{10.109}$$

where the Dirac delta-function enforces conservation of the particle rest mass m. The 4-volume d^4p is a scalar, and the delta-function is a function of a scalar argument, hence d^3p/E is likewise a scalar. Since $E\, d^3r$ and d^3p/E are both Lorentz-invariant scalars, so is their product, the phase space volume $d^3r\, d^3p$.

10.26.2 Occupation number in a FLRW universe

The homogeneity and isotropy of a FLRW universe imply that, for a comoving observer, the occupation number f is independent of position and direction,

$$f(x^\mu, \boldsymbol{p}) \ = f(p)\ . \tag{10.110}$$

[1] A more rigorous approach to this kind of argument can be found in Chapter 15. In fact $E\, d^3r = p^0\, dr^1 \wedge dr^2 \wedge dr^3$ is a pseudoscalar, not a scalar, which explains the restriction here to a locally inertial frame.

10.26.3 Number density

In the locally inertial frame of an observer, the number density and flux of a particle species form a 4-vector n^k,

$$n^k = \int p^k \, f(x^\mu, \boldsymbol{p}) \, \frac{d^3p}{E(2\pi\hbar)^3} \ . \tag{10.111}$$

In a FLRW universe, the spatial components of the number flux vanish by isotropy, so the only non-vanishing component is the time component n^0, which is just the proper number density n of the particle species,

$$n \equiv n^0 = \int f(p) \, \frac{4\pi p^2 dp}{(2\pi\hbar)^3} \ . \tag{10.112}$$

10.26.4 Energy-momentum tensor

In the locally inertial frame of an observer, the energy-momentum tensor T_{kl} of a particle species is

$$T_{kl} = \int p_k p_l \, f(x^\mu, \boldsymbol{p}) \, \frac{d^3p}{E(2\pi\hbar)^3} \ . \tag{10.113}$$

For a FLRW universe, homogeneity and isotropy imply that the energy-momentum tensor in the locally inertial frame of a comoving observer is diagonal, with time component $T_{00} = \rho$, and isotropic spatial components $T_{ab} = p \, \delta_{ab}$. The proper energy density ρ of a particle species is

$$\rho = \int E \, f(p) \, \frac{4\pi p^2 dp}{(2\pi\hbar)^3} \ , \tag{10.114}$$

and the proper isotropic pressure p is (don't confuse pressure p on the left hand side with momentum p on the right hand side)

$$p = \int \frac{p^2}{3E} f(p) \, \frac{4\pi p^2 dp}{(2\pi\hbar)^3} \ . \tag{10.115}$$

Exercise 10.12 Distribution of non-interacting particles initially in thermodynamic equilibrium. The number dN of a particle species in an interval $d^3r d^3p$ of phase space (proper positions r and proper momenta p, not to be confused with the same symbol p for pressure) for an ideal gas of free particles (non-relativistic, relativistic, or anything in between) in thermodynamic equilibrium at temperature T and chemical potential μ is

$$dN = f \, \frac{d^3r d^3p}{(2\pi\hbar)^3} \ , \tag{10.116}$$

where the occupation number f is (units $c = k = 1$, where k is the Boltzmann factor)

$$f = \frac{1}{e^{(E-\mu)/T} \pm 1} \ , \tag{10.117}$$

with a + sign for fermions and a − sign for bosons. The energy E and momentum p of particles of mass m are related by $E^2 = p^2 + m^2$. For bosons, the chemical potential is constrained to satisfy $\mu \leq E$, but for fermions μ may take any positive or negative value, with $\mu \gg E$ corresponding to a degenerate Fermi gas. As the Universe expands, proper distance increase as $r \propto a$, while proper momenta decrease as $p \propto a^{-1}$, so the phase space volume $d^3r d^3p$ remains constant.

1. **Occupation number.** Write down an expression for the occupation number $f(p)$ of a distribution of particles that start in thermodynamic equilibrium and then remain non-interacting while the Universe expands by a factor a.
2. **Relativistic particles.** Conclude that a distribution of non-interacting relativistic particles initially in thermodynamic equilibrium retains its thermodynamic equilibrium distribution in a FLRW universe as long as the particles remain relativistic. How do the temperature T and chemical potential μ of the relativistic distribution vary with cosmic scale factor a?
3. **Non-relativistic particles.** Show similarly that a distribution of non-interacting non-relativistic particles initially in thermodynamic equilibrium remains thermal. How do the temperature T and chemical potential $\mu - m$ of the non-relativistic distribution vary with cosmic scale factor a?
4. **Transition from relativistic to non-relativistic.** What happens to a distribution of non-interacting particles that are relativistic in thermodynamic equilibrium, but redshift to being non-relativistic?

Exercise 10.13 The first law of thermodynamics with non-conserved particle number. As seen in §10.9.2, the first law of thermodynamics in the form

$$T\, d(a^3 s) = d(a^3 \rho) + p\, d(a^3) = 0 \tag{10.118}$$

is built into Friedmann's equations. But what happens when for example the temperature falls through the temperature $T \approx 0.5\,\mathrm{MeV}$ at which electrons and positrons annihilate? Won't there be entropy production associated with $e\bar{e}$ annihilation? Should not the first law of thermodynamics actually say

$$T\, d(a^3 s) = d(a^3 \rho) + p\, d(a^3) - \sum_X \mu_X\, d(a^3 n_X)\ , \tag{10.119}$$

with the last term taking into account the variation in the number $a^3 n_X$ of various species X?

Solution. Each distinct chemical potential μ_X is associated with a conserved number, so the additional terms contribute zero change to the entropy,

$$\sum_X \mu_X\, d(a^3 n_X) = 0\ , \tag{10.120}$$

as long as the species are in mutual thermodynamic equilibrium. For example, positrons and electrons in thermodynamic equilibrium satisfy $\mu_{\bar{e}} = -\mu_e$, and

$$\mu_e\, d(a^3 n_e) + \mu_{\bar{e}}\, d(a^3 n_{\bar{e}}) = \mu_e\, d(a^3 n_e - a^3 n_{\bar{e}}) = 0\ , \tag{10.121}$$

which vanishes because the difference $a^3 n_e - a^3 n_{\bar{e}}$ between electron and positron number is conserved. Thus the entropy conservation equation (10.118) remains correct in a FLRW universe even when number changing processes are occurring.

Exercise 10.14 Number, energy, pressure, and entropy of a relativistic ideal gas at zero chemical potential. The number density n, energy density ρ, and pressure p of an ideal gas of a single species of free particles are given by equations (10.112), (10.114), and (10.115), with occupation number (10.117). Show that for an ideal relativistic gas of g bosonic species in thermodynamic equilibrium at temperature T and zero chemical potential, $\mu = 0$, the number density n, energy density ρ, and pressure p are (units $c = k = 1$; number density n in units 1/volume, energy density ρ and pressure p in units energy/volume)

$$n = g\frac{\zeta(3)T^3}{\pi^2\hbar^3} \ , \quad \rho = 3p = g\frac{\pi^2 T^4}{30\hbar^3} \ , \tag{10.122}$$

where $\zeta(3) = 1.2020569$ is a Riemann zeta function. The entropy density s of an ideal gas of free particles in thermodynamic equilibrium at zero chemical potential is

$$s = \frac{\rho + p}{T} \ . \tag{10.123}$$

Conclude that the entropy density s of an ideal relativistic gas of g bosonic species in thermodynamic equilibrium at temperature T and zero chemical potential is (units 1/volume)

$$s = g\frac{2\pi^2 T^3}{45\hbar^3} \ . \tag{10.124}$$

Exercise 10.15 A relation between thermodynamic integrals. Prove that

$$\int_0^\infty \frac{x^{n-1}\,dx}{e^x + 1} = \left(1 - 2^{1-n}\right)\int_0^\infty \frac{x^{n-1}\,dx}{e^x - 1} \ . \tag{10.125}$$

[Hint: Use the fact that $(e^x + 1)(e^x - 1) = (e^{2x} - 1)$.] Hence argue that the ratios of number, energy, and entropy densities of relativistic fermionic (f) to relativistic bosonic (b) species in thermodynamic equilibrium at the same temperature are

$$\frac{n_{\rm f}}{n_{\rm b}} = \frac{3}{4} \ , \quad \frac{\rho_{\rm f}}{\rho_{\rm b}} = \frac{s_{\rm f}}{s_{\rm b}} = \frac{7}{8} \ . \tag{10.126}$$

Conclude that if the number n, energy ρ, and entropy s of a mixture of bosonic and fermioni species in thermodynamic equilbrium at the same temperature T are written in the form of equations (10.122) and (10.124), then the effective number-, energy-, and entropy-weighted numbers g of particle species are, in terms of the number $g_{\rm b}$ of bosonic and $g_{\rm f}$ of fermionic species,

$$g_n = g_{\rm b} + \frac{3}{4}g_{\rm f} \ , \quad g_\rho = g_s = g_{\rm b} + \frac{7}{8}g_{\rm f} \ . \tag{10.127}$$

Exercise 10.16 Relativistic particles in the early Universe had approximately zero chemical potential. Show that the small particle-antiparticle symmetry of our Universe implies that to a good approximation relativistic particles in thermodynamic equilibrium in the early Universe had zero chemical potential.

Solution. The chemical potentials of particles X and antiparticles $\bar{X}$ in thermodynamic equilibrium are necessarily related by

$$\mu_{\bar{X}} = -\mu_X \ . \tag{10.128}$$

If the particle-antiparticle asymmetry is denoted η, defined for relativistic particles by

$$n_X - n_{\bar{X}} = \eta\, n_X \ , \tag{10.129}$$

then $\mu_X/T \sim \eta$. More accurately, to linear order in η,

$$\frac{\mu_X}{T} \approx \eta\, \frac{\pi^2}{3\,\zeta(3)} \times \begin{cases} 1 & \text{(bosons)} \\ \frac{2}{3} & \text{(fermions)} \end{cases} \ . \tag{10.130}$$

Exercise 10.17 Entropy per particle. The entropy of an ideal gas of free particles in thermodynamic equilibrium is

$$s = \frac{\rho + p - \mu n}{T} \ . \tag{10.131}$$

Argue that the entropy per particle s/n is a quantity of order unity, whether particles are relativistic or non-relativistic.

Solution. For relativistic bosons with zero chemical potential, equations (10.122) and (10.124) imply that the entropy per particle is

$$\frac{s}{n} = \frac{2\pi^4}{45\zeta(3)} \times \begin{cases} 1 & = 3.6 \quad \text{(bosons)} \ , \\ \frac{7}{6} & = 4.2 \quad \text{(fermions)} \ . \end{cases} \tag{10.132}$$

For a non-relativistic species, the number density n is related to the temperature T and chemical potential μ by

$$n = \left(\frac{mT}{2\pi\hbar^2}\right)^{3/2} e^{(\mu - m)/T} \ . \tag{10.133}$$

Under cosmological conditions, the occupation number of non-relativistic species was small, $e^{(\mu-m)/T} \ll 1$. However, tiny occupation numbers correspond to values of $(\mu - m)/T$ that are only logarithmically large (negative). The entropy per particle of a non-relativistic species is

$$\frac{s}{n} = \frac{5}{2} + \ln\left[\frac{1}{n}\left(\frac{mT}{2\pi\hbar^2}\right)^{3/2}\right] \ , \tag{10.134}$$

which remains modest even if the argument of the logarithm is huge.

Exercise 10.18 Photon temperature at high redshift versus today. Use entropy conservation, $a^3 s =$ constant, to argue that the ratio of the photon temperature T at redshift z in the early Universe to the photon temperature T_0 today is as given by equation (10.98).

Exercise 10.19 Cosmic Neutrino Background.

1. **Temperature of the CNB.** Weak interactions were fast enough to keep neutrinos in thermodynamic equilibrium with protons and neutrons, hence with photons, electrons, and positrons up to just before $e\bar{e}$ annihilation, but then neutrinos decoupled. When electrons and positrons annihilated, they dumped

their entropy into that of photons, leaving the entropy of neutrinos unchanged. Argue that conservation of comoving entropy implies

$$a^3 T^3 \left(g_\gamma + \frac{7}{8} g_e \right) = T_\gamma^3 \, g_\gamma \ , \tag{10.135a}$$

$$a^3 T^3 \, g_\nu = T_\nu^3 \, g_\nu \ , \tag{10.135b}$$

where the left hand sides refer to quantities before $e\bar{e}$ annihilation, which happened at $T \sim 0.5\,\mathrm{MeV}$, and the right hand sides to quantities after $e\bar{e}$ annihilation (including today). Deduce the ratio of neutrino to photon temperatures today,

$$\frac{T_\nu}{T_\gamma} \ . \tag{10.136}$$

Does the temperature ratio (10.136) depend on the number of neutrino types? What is the neutrino temperature today in K, if the photon temperature today is 2.725 K?

2. **Effective number of relativistic particle species.** Because the temperatures of photons and neutrinos are different, the effective number g of relativistic species today is not given by equations (10.127). What are the effective number-, energy-, and entropy-weighted numbers $g_{n,0}$, $g_{\rho,0}$, and $g_{s,0}$ of relativistic particle species today? What are their arithmetic values if the relativistic species consist of photons and three species of neutrino? How are these values altererd if, as is likely, neutrinos today are non-relativistic?

Solution. The ratio of neutrino to photon temperatures after $e\bar{e}$ annihilation is

$$\frac{T_\nu}{T_\gamma} = \left(\frac{g_\gamma}{g_\gamma + \frac{7}{8} g_e} \right)^{1/3} = \left(\frac{4}{11} \right)^{1/3} = 0.714 \ . \tag{10.137}$$

No, the temperature ratio does not depend on the number of neutrino types. The ratio depends on neutrinos having decoupled a short time before $e\bar{e}$-annihilation. Equation (10.137) implies that the CNB temperature is given by equation (10.99). With 2 bosonic degrees of freedom from photons, and 6 fermionic degrees of freedom from 3 relativistic neutrino types, the effective number-, energy-, and entropy-weighted number of relativistic degrees of freedom is

$$g_{n,0} = g_\gamma + \left(\frac{T_\nu}{T_\gamma} \right)^3 \frac{3}{4} \, g_\nu = 2 + \frac{4}{11} \frac{3}{4} 6 = \frac{40}{11} = 3.64 \ , \tag{10.138a}$$

$$g_{\rho,0} = g_\gamma + \left(\frac{T_\nu}{T_\gamma} \right)^4 \frac{7}{8} \, g_\nu = 2 + \left(\frac{4}{11} \right)^{4/3} \frac{7}{8} 6 = 3.36 \ , \tag{10.138b}$$

$$g_{s,0} = g_\gamma + \left(\frac{T_\nu}{T_\gamma} \right)^3 \frac{7}{8} \, g_\nu = 2 + \frac{4}{11} \frac{7}{8} 6 = \frac{43}{11} = 3.91 \ . \tag{10.138c}$$

Neutrinos today interact too weakly to annihilate, so their number and entropy today is that of relativistic species even if they are non-relativistic today. However, their energy density today is not that of relativistic particles.

Exercise 10.20 Sterile Neutrinos. An active neutrino (ν) is one that interacts by weak interactions, while a sterile neutrino ($\not{\nu}$) is one that does not. Suppose that the 3 active left-handed neutrino types have sterile right-handed partners of the same mass. This would necessarily be the case if neutrinos are Dirac neutrinos (as opposed to Majorana neutrinos). Assume that the active neutrinos can oscillate into each other, but active and sterile neutrinos cannot oscillate into each other. Suppose that left- and right-handed neutrinos were in equal abundance above the electroweak temperature 100 GeV, perhaps as a result of being in mutual thermodynamic equilibrium at some earlier time. What is the ratio $T_{\not{\nu}}/T_\nu$ of sterile to active neutrino temperatures at the time of recombination? What is the entropy-weighted effective number of relativistic species at recombination?

Solution. Active neutrinos remain in thermodynamic equilibrium until they decouple at $T \sim 1\,\text{MeV}$. Thus Standard Model particles that become non-relativistic between 100 GeV and 1 MeV dump their entropy into active neutrinos (and photons and electrons), but not into sterile neutrinos. The equations governing conservation of entropy for active neutrinos and sterile neutrinos are

$$a^3 T^3 \left(g_\text{b} + \frac{7}{8}\, g_\text{f} \right)_{T \sim 100\,\text{GeV}} = T_\nu^3 \left(g_\text{b} + \frac{7}{8}\, g_\text{f} \right)_{T \sim 1\,\text{MeV}} , \tag{10.139a}$$

$$a^3 T^3 \, \frac{7}{8}\, g_{\not{\nu}} = T_{\not{\nu}}^3 \, \frac{7}{8}\, g_{\not{\nu}} , \tag{10.139b}$$

where from Table 10.4 the effective number of bosonic and fermionic types, excluding sterile neutrinos, is $g_\text{b} = 2 \times 14$ and $g_\text{f} = 2 \times 45$ at $T \sim 100\,\text{GeV}$, and $g_\text{b} = 2 \times 1$ and $g_\text{f} = 2 \times 5$ at $T \sim 1\,\text{MeV}$, and the number of sterile neutrino types is $g_{\not{\nu}} = 2 \times 3$. Hence the ratio $T_{\not{\nu}}/T_\nu$ of sterile to active neutrino temperatures at $T \sim 1\,\text{MeV}$ is

$$\frac{T_{\not{\nu}}}{T_\nu} = \left(\frac{1 + \frac{7}{8}\, 5}{14 + \frac{7}{8}\, 45} \right)^{1/3} = \left(\frac{43}{427} \right)^{1/3} = 0.465 . \tag{10.140}$$

This ratio is preserved thereafter, since active and sterile neutrinos are both decoupled below 1 MeV. The entropy-weighted effective number of relativistic species at recombination is

$$2 \left[1 + \frac{7}{8}\, \frac{4}{11} \left(3 + \frac{43}{427}\, 3 \right) \right] = 4.10 . \tag{10.141}$$

The effective number N_eff of neutrino species would be

$$N_\text{eff} = 3 + \frac{43}{427}\, 3 = 3.30 , \tag{10.142}$$

in good agreement with the value inferred from observations with the Planck satellite Ade (2013),

$$N_\text{eff} = 3.30 \pm 0.27 . \tag{10.143}$$

10.27 Maximally symmetric spaces

By construction, the FLRW metric is spatially homogeneous and isotropic, which means it has maximal spatial symmetry. A special subclass of FLRW metrics is in addition stationary, satisfying time translation invariance. As you will show in Exercise 10.21, stationary FLRW metrics may have curvature and a cosmological constant, but no other source. You will also show that a coordinate transformation brings such FLRW metrics to the explicitly stationary form

$$ds^2 = -\left(1 - \tfrac{1}{3}\Lambda r^2\right) dt_{\rm s}^2 + \frac{dr_s^2}{1 - \frac{1}{3}\Lambda r^2} + r_s^2\, do^2 \ , \tag{10.144}$$

where the time $t_{\rm s}$ and radius $r_{\rm s}$ are subscripted s for stationary to distinguish them from FLRW time t and radius r.

Spacetimes that are homogeneous, isotropic, and stationary, and are therefore described by the metric (10.144), are called **maximally symmetric**. A maximally symmetric space with a positive cosmological constant, $\Lambda > 0$, is called **de Sitter** (dS) space, while that with a negative cosmological constant, $\Lambda < 0$, is called **anti de Sitter** (AdS) space. The maximally symmetric space with zero cosmological constant is just Minkowski space. Thanks to their high degree of symmetry, de Sitter and anti de Sitter spaces play a prominent role in theoretical studies of quantum gravity.

de Sitter space has a horizon at radius $r_{\rm H} = \sqrt{3/\Lambda}$. Whereas inside the horizon the time coordinate $t_{\rm s}$ is timelike and the radial coordinate $r_{\rm s}$ is spacelike, outside the horizon the time coordinate $t_{\rm s}$ is spacelike and the radial coordinate $r_{\rm s}$ is timelike.

The Riemann tensor, Ricci tensor, Ricci scalar, and Einstein tensor of maximally symmetric spaces are

$$R_{\kappa\lambda\mu\nu} = \tfrac{1}{3}\Lambda(g_{\kappa\mu}g_{\lambda\nu} - g_{\kappa\nu}g_{\lambda\mu}) \ , \quad R_{\kappa\mu} = \Lambda g_{\kappa\mu} \ , \quad R = 4\Lambda \ , \quad G_{\kappa\mu} = -\Lambda g_{\kappa\mu} \ . \tag{10.145}$$

10.27.1 de Sitter spacetime as a closed FLRW spacetime

Just as it was possible to conceive the spatial part of the FLRW geometry as a 3D hypersphere embedded in 4D Euclidean space, §10.6, so also it is possible to conceive a maximally symmetric space as a 4D hyperboloid embedded in 5D space.

For de Sitter space, the parent 5D space is a Minkowski space with metric $ds^2 = -du^2 + dx^2 + dy^2 + dz^2 + dw^2$, and the embedded 4D hyperboloid is a set of points

$$-u^2 + x^2 + y^2 + z^2 + w^2 = r_{\rm H}^2 = \text{constant} \ , \tag{10.146}$$

with $r_{\rm H}$ the horizon radius

$$r_{\rm H} = \sqrt{\frac{3}{\Lambda}} \ . \tag{10.147}$$

The de Sitter hyperboloid is illustrated in Figure 10.14. Let $r \equiv (x^2 + y^2 + z^2)^{1/2}$, and introduce the boost

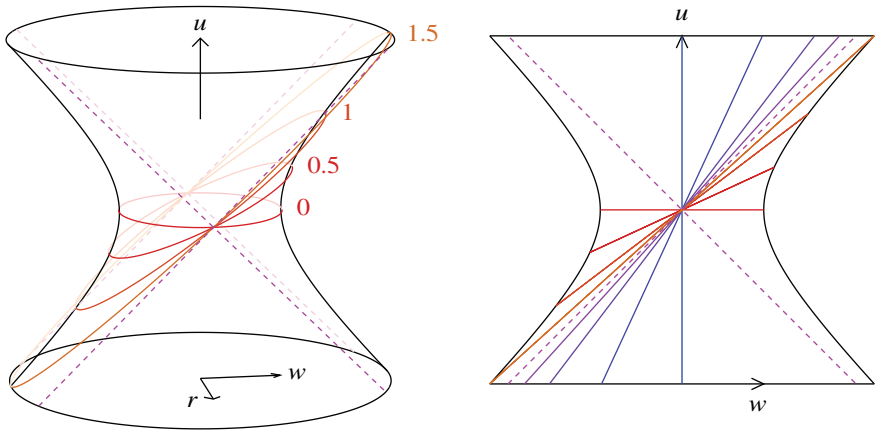

Figure 10.14 Embedding spacetime diagram of de Sitter space, shown on the left in 3D, on the right in a 2D projection on to the u-w plane. Objects are confined to the surface of the embedded hyperboloid. The vertical direction is timelike, while the horizontal directions are spacelike. The position of a non-accelerating observer defines a "north pole" at $r = 0$ and $w > 0$, traced by the (black) line at the right edge of each diagram. Antipodeal to the north pole is a "south pole" at $r = 0$ and $w < 0$, traced by the (black) line at the left edge of each diagram. The (reddish) skewed circles on the 3D diagram, which project to straight lines in the 2D diagram, are lines of constant stationary time t_s, labelled with their value in units of the horizon radius r_H, as measured by the observer at rest at the north pole $r = 0$. Lines of constant stationary time t_s transform into each other under a Lorentz boost in the u–w plane. The 45° dashed lines are null lines constituting the past and future horizons of the north pole observer (or of the south pole observer). The 2D diagram on the right shows in addition a sample of (bluish) timelike geodesics that pass through $u = w = 0$ (these lines are omitted from the 3D diagram).

angle ψ and rotation angle χ defined by

$$u = r_H \sinh\psi \ , \tag{10.148a}$$

$$r = r_H \cosh\psi \sin\chi \ , \tag{10.148b}$$

$$w = r_H \cosh\psi \cos\chi \ . \tag{10.148c}$$

The radius r defined by equation (10.148b) is the same as the radius r_s in the stationary metric (10.144). In terms of the angles ψ and χ, the metric on the de Sitter 4D hyperboloid is

$$ds^2 = r_H^2 \left[-d\psi^2 + \cosh^2\psi \left(d\chi^2 + \sin^2\chi \, do^2 \right) \right] \ . \tag{10.149}$$

The metric (10.149) is of FLRW form (10.26) with $t = r_H\psi$ and $a(t) = \kappa^{1/2} r_H \cosh\psi$, and a closed spatial geometry. The de Sitter space describes a spatially closed FLRW universe that contracts, reaches a minimum size at $t = 0$, then reexpands. Comoving observers, those with $\chi =$ constant and fixed angular position, move vertically upward on the embedded hyperboloid in Figure 10.14.

The spatial position at $r = 0$ and $w > 0$ defines a "north pole" of de Sitter space. Antipodeal to the north

pole is a "south pole" at $r = 0$ and $w < 0$. The surface $u = w$ is a future horizon for an observer at the north pole, and a past horizon for an observer at the south pole. Similarly the surface $u = -w$ is a past horizon for an observer at the north pole, and a future horizon for an observer at the south pole. The causal diamond of any observer is the region of spacetime bounded by the observer's past and future horizons. The north polar observer's causal diamond is the region $w > |u|$, while the south polar observer's causal diamond is the region $w < -|u|$.

The radial coordinate r is spacelike within the causal diamonds of either the north or south polar observers, where $|w| > |u|$, but timelike outside those causal diamonds, where $|w| < |u|$.

The de Sitter hyperboloid possesses a symmetry under Lorentz boosts in the u–w plane. The time t_s in the stationary metric (10.144) is, modulo a factor of r_H, the boost angle of this Lorentz boost, which is

$$t_s = \begin{cases} r_H \tanh^{-1}(u/w) & |w| > |u| \ , \\ r_H \tanh^{-1}(w/u) & |w| < |u| \ . \end{cases} \tag{10.150}$$

The stationary time coordinate t_s is timelike inside the causal diamonds of either the north or south pole observers, $|w| > |u|$, but spacelike outside those causal diamonds, $|w| < |u|$.

10.27.2 de Sitter spacetime as an open FLRW spacetime

An alternative coordinatization of the same embedded hyperboloid (10.146) for de Sitter space yields a metric in FLRW form but with an open spatial geometry. Let $r \equiv (x^2 + y^2 + z^2)^{1/2}$ as before, and define ψ and χ by

$$u = r_H \sinh\psi \cosh\chi \ , \tag{10.151a}$$

$$r = r_H \sinh\psi \sinh\chi \ , \tag{10.151b}$$

$$w = r_H \cosh\psi \ . \tag{10.151c}$$

The r defined by equation (10.151b) is *not* the same as the r_s in the stationary metric (10.144); rather, it is w that equals r_s. In terms of the angles ψ and χ defined by equations (10.151), the metric on the de Sitter 4D hyperboloid is

$$ds^2 = r_H^2 \left[-d\psi^2 + \sinh^2\psi \left(d\chi^2 + \sinh^2\chi \, do^2 \right) \right] \ . \tag{10.152}$$

The metric (10.152) is in FLRW form (10.26) with $t = r_H\psi$ and $a(t) = (-\kappa)^{1/2} r_H \sinh\psi$, and an open spatial geometry. Whereas the coordinates $\{\psi, \chi\}$, equation (10.148), for de Sitter with closed spatial geometry cover the entire embedded hyperboloid shown in Figure 10.14, the coordinates $\{\psi, \chi\}$, equation (10.151), for de Sitter with open spatial geometry cover only the region of the hyperboloid with $|u| \geq |r|$ and $w \geq r_H$. The region of positive cosmic scale factor, $\psi \geq 0$, corresponds to $u \geq 0$. Conceptually, for de Sitter with open spatial geometry, there is a Big Bang at $\{u, r, w\} = \{0, 0, 1\} r_H$, comoving observers from which fill the region $u \geq |r|$ and $w \geq r_H$. Comoving observers, those with $\chi =$ constant, follow straight lines in the u–r plane, bounded by the null cone at $u = |r|$.

In the open FLRW metric (10.152) for de Sitter space, the coordinates t_s and r_s of the stationary metric (10.144) are respectively spacelike and timelike. Lines of constant stationary time t_s, equation (10.150),

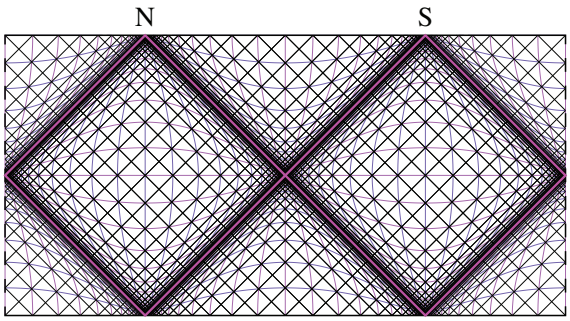

Figure 10.15 Penrose diagram of de Sitter space. The left and right edges are identified. The topology is that of a 3-sphere in the horizontal (spatial) direction times the real line in the vertical (time) direction. The thick (pink) null lines are past and future horizons for observers who follow (vertical) geodesics at the "north" and "south" poles at $r = 0$, marked N and S. The horizontal and vertical contours are contours of constant stationary time t_s and radius r_s in the stationary form (10.144) of the de Sitter metric. The contours are uniformly spaced by 0.4 in t_s/r_H and the tortoise coordinate r_s^*/r_H, equation (10.165). The stationary coordinates t_s and r_s are respectively timelike and spacelike inside the causal diamonds of the north and south pole observers, but switch to being respectively spacelike and timelike outside the causal diamonds, in the lower and upper wedges. The lower and upper wedges correspond to the open FLRW version (10.152) of the de Sitter metric. In the lower wedges, comoving observers collapse to a Big Crunch where their future horizons converge, while in the upper wedges, comoving observers expand away from a Big Bang from which their past horizons diverge.

coincide with geodesics of comoving observers, at constant χ, while lines of constant stationary radius $r_s = w$, equation (10.151c), coincide with lines of constant FLRW time ψ,

$$t_s/r_H = \chi \ , \tag{10.153a}$$

$$r_s/r_H = w/r_H = \cosh\psi \ . \tag{10.153b}$$

10.27.3 Penrose diagram of de Sitter space

Figure 10.15 shows a Penrose diagram of de Sitter space. A natural choice of Penrose coordinates comes from requiring that vertical lines on the embedded de Sitter hyperboloid 10.14 become vertical lines on the Penrose diagram. These vertical lines are geodesics for comoving observers, lines of constant χ, in the closed FLRW form (10.149) form of the de Sitter metric. The corresponding Penrose time coordinate t_P follows from solving for the radial null geodesics of the metric (10.149), whence $t_P = \int d\psi/\cosh\psi$. The resulting Penrose coordinates for de Sitter space are

$$t_P = \tan^{-1}(\sinh\psi) = \tan^{-1}(u/r_H) \ , \tag{10.154a}$$

$$r_P = \chi = \tan^{-1}(r/w) \ . \tag{10.154b}$$

The radial coordinate r in both the closed and open FLRW forms (10.149) and (10.152) of the de Sitter

metric was chosen so that a comoving observer at the origin was at $r = 0$, at either the north or the south pole. The Penrose diagram 10.15 depicts both closed and open FLRW geometries, but the open geometry is shifted by 90° to the equator, so that it appears to interleave with the closed geometry instead of overlapping it. The thick (pink) null lines at 45° outline the causal diamonds of north and south polar observers in the closed FLRW geometry. The null lines also outline the causal wedges of equatorial observers in the open FLRW geometry. The lower wedges correspond to collapsing spacetimes that terminate in a Big Crunch where the null lines cross. The upper wedges correspond to expanding spacetimes that begin in a Big Bang where the null lines cross. Note that the causal diamonds of any non-accelerating observer are spherically symmetric about the observer. Thus the causal diamonds of the closed and open observers touch only along one-dimensional lines, not along three-dimensional hypersurfaces as the Penrose diagram might suggest. The causal diamonds of observers in de Sitter and anti de Sitter spacetimes are different for different observers, and there is no reason to expect that the spacetime could be tiled fully by the causal diamonds of some set of observers.

There is no physical singularity, no divergence of the Riemann tensor, at the Big Crunch and Big Bang points of the collapsing and expanding open FLRW forms of the de Sitter geometry. Does that mean that the collapsing de Sitter spacetime evolves smoothly into an expanding spacetime? As long as the spacetime is pure vacuum, there is no way to tell whether spacetime is expanding or collapsing. Only when the spacetime contains matter of some kind, as our Universe does, can a preferred set of comoving coordinates be defined. When matter is present, Big Crunches and Big Bangs are, setting aside quantum gravity, genuine singularities that cannot be removed by a coordinate transformation.

The horizontal and vertical contours in the Penrose diagram 10.15 are contours of constant stationary time $t_{\rm s}$ and radius $r_{\rm s}$. Translation in $t_{\rm s}$ is a symmetry of de Sitter spacetime, and to exhibit this symmetry, the contours of $t_{\rm s}$ in the Penrose diagram are chosen to be uniformly spaced. A similarly symmetric appearance for the radial coordinate is achieved by choosing contours of $r_{\rm s}$ to be uniformly spaced in the tortoise coordinate $r^*_{\rm s}$

$$r^*_{\rm s} \equiv \int \frac{dr_{\rm s}}{1 - r_{\rm s}^2/r_{\rm H}^2} = r_{\rm H} \tanh^{-1}(r_{\rm s}/r_{\rm H}) \ . \tag{10.155}$$

The contours in the Penrose diagram 10.15 are uniformly spaced by 0.4 in $t_{\rm s}/r_{\rm H}$ and $r^*_{\rm s}/r_{\rm H}$. In terms of the time and tortoise coordinates t_s and $r^*_{\rm s}$, the Penrose time and radial coordinates are

$$t_{\rm P} \pm r_{\rm P} = \tan^{-1}\left[\sinh\left(\frac{t_{\rm s} \pm r^*_{\rm s}}{r_{\rm H}}\right)\right] \ . \tag{10.156}$$

10.27.4 Anti de Sitter space

For anti de Sitter space, the parent 5D space is a Minkowski space with signature $--+++$, metric $ds^2 = -du^2 - dv^2 + dx^2 + dy^2 + dz^2$, and the embedded 4D hyperboloid is a set of points

$$-u^2 - v^2 + x^2 + y^2 + z^2 = -r_{\rm H}^2 = \text{constant} \ , \tag{10.157}$$

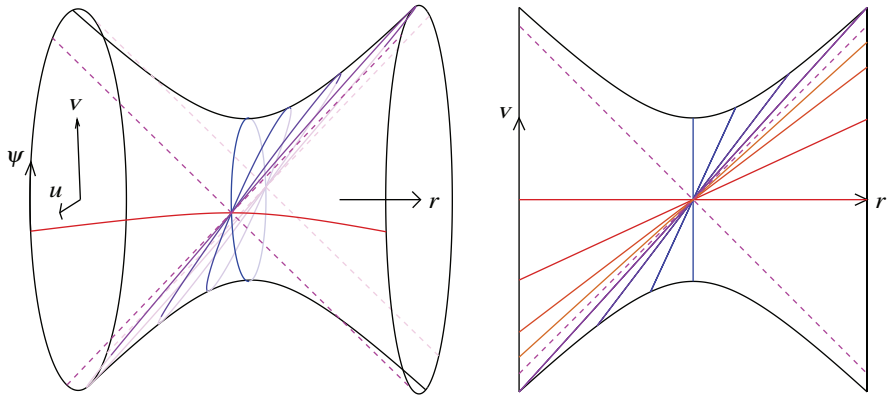

Figure 10.16 Embedding spacetime diagram of anti de Sitter space, shown on the left in 3D, on the right in a 2D projection on to the v-r plane. The vertical direction winding around the hyperboloid is timelike, while the horizontal direction is spacelike. The position of a non-accelerating observer defines a spatial "pole" at $r = 0$. In the 3D diagram, the (red) horizontal line is an example line of constant stationary time t_s for the observer at the pole. Lines of constant stationary time t_s transform into each other under a rotation in the u–v plane. The (bluish) lines at less than 45° from vertical are a sample of geodesics that pass through the pole at $r = 0$ at time $\psi = 0$. In anti de Sitter space, all timelike geodesics that pass through a spatial point boomerang back to the spatial point in a proper time πr_H. The 2D diagram on the right shows in addition (reddish) lines of constant stationary time t_s for observers on the various geodesics.

with $r_\mathrm{H} \equiv \sqrt{-3/\Lambda}$. The anti de Sitter hyperboloid is illustrated in Figure 10.16. Let $r \equiv (x^2 + y^2 + z^2)^{1/2}$, and introduce the boost angle χ and rotation angle ψ defined by

$$u = r_\mathrm{H} \cosh\chi \cos\psi \ , \tag{10.158a}$$

$$v = r_\mathrm{H} \cosh\chi \sin\psi \ , \tag{10.158b}$$

$$r = r_\mathrm{H} \sinh\chi \ . \tag{10.158c}$$

The time coordinate ψ defined by equations (10.158) appears to be periodic, with period 2π, but this is an artefact of the embedding. In a causal spacetime, the time coordinate would not loop back on itself. Rather, the coordinate ψ can be taken to increase monotonically as it loops around the hyperboloid, extending from $-\infty$ to ∞. In terms of the angles ψ and χ, the metric on the anti de Sitter 4D hyperboloid is

$$ds^2 = r_\mathrm{H}^2 \left(-\cosh^2\chi \, d\psi^2 + d\chi^2 + \sinh^2\chi \, do^2 \right) \ . \tag{10.159}$$

The metric (10.159) is of stationary form (10.144) with $t_\mathrm{s} = r_\mathrm{H}\psi$ and $r = r_\mathrm{H} \sinh\chi$.

10.27.5 Anti de Sitter spacetime as an open FLRW spacetime

An alternative coordinatization of the same embedded hyperboloid 10.16 for anti de Sitter space,

$$u = r_{\rm H} \cos\psi \ , \tag{10.160a}$$
$$v = r_{\rm H} \sin\psi \cosh\chi \ , \tag{10.160b}$$
$$r = r_{\rm H} \sin\psi \sinh\chi \ . \tag{10.160c}$$

yields a metric in FLRW form with an open spatial geometry,

$$ds^2 = r_{\rm H}^2 \left[- d\psi^2 + \sin^2\psi (d\chi^2 + \sinh^2\chi \, do^2) \right] \ . \tag{10.161}$$

Whereas the coordinates (10.158) cover all of the anti de Sitter hyperboloid 10.16, the open coordinates (10.160) cover only the regions with $|u| \leq r_{\rm H}$. These are the upper and lower diamonds bounded by the (pink) dashed null lines in the hyperboloid 10.16. In each diamond, the open spacetime undergoes a Big Bang at the earliest vertex of the diamond, expands to a maximum size, turns around, and collapses to a Big Crunch at the latest vertex of the diamond.

10.27.6 Anti de Sitter spacetime as a Rindler space

Anti de Sitter spacetime possesses symmetry under Lorentz boosts in any time-space plane, such as the v–x plane. In the open FLRW form (10.161) of anti de Sitter geometry, such boosts transform geodesics of comoving observers into each other. Outside the open causal diamonds on the other hand, these boosts generate the worldlines of a certain set of "Rindler" observers who accelerate with constant acceleration in the v–x plane. Rindler time and space coordinates $\{\chi, \psi\}$ are defined by

$$u = r_{\rm H} \cosh\psi \ , \tag{10.162a}$$
$$v = r_{\rm H} \sinh\psi \sinh\chi \ , \tag{10.162b}$$
$$x = r_{\rm H} \sinh\psi \cosh\chi \ , \tag{10.162c}$$

yielding the AdS Rindler metric

$$ds^2 = r_{\rm H}^2 \left(- \sinh^2\psi \, d\chi^2 + d\psi^2 \right) + dy^2 + dz^2 \ . \tag{10.163}$$

10.27.7 Penrose diagram of anti de Sitter space

Figure 10.17 shows a Penrose diagram of anti de Sitter space. A natural choice of Penrose coordinates comes from requiring that horizontal lines on the embedded anti de Sitter hyperboloid 10.16 become horizontal lines on the Penrose diagram. These horizontal lines are lines of constant stationary time $t_{\rm s} = r_{\rm H}\psi$ in the stationary form (10.159) form of the anti de Sitter metric. The corresponding Penrose radial coordinate $r_{\rm P}$

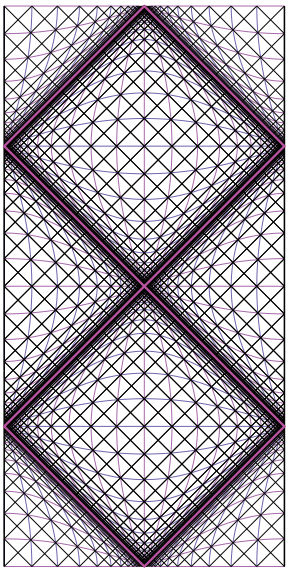

Figure 10.17 Penrose diagram of anti de Sitter space. The diagram repeats vertically indefinitely. The topology is that of Euclidean 3-space in the horizontal (spatial) direction times the real line in the vertical (time) direction. The thick (pink) null lines outline the causal diamonds of observers in the open FLRW form (10.161) of the anti de Sitter spacetime. The spacetime of the open FLRW geometry expands from a Big Bang at a crossing point of the null lines, and collapses to a Big Crunch at the next crossing point. The thick null lines also outline the causal wedges of Rindler observers, equation (10.163), at the left and right edges of the diagram. The horizontal and vertical contours are lines of constant ψ and χ, uniformly spaced by 0.4 in χ and ψ^*, equation (10.166), in both the open FLRW diamonds and in the left and right Rindler wedges, equations (10.161) and (10.163). The coordinates ψ and χ are resepectively timelike and spacelike in the open diamonds, and respectively spacelike and timelike in the Rindler wedges.

follows from solving for the radial null geodesics of the metric (10.159), whence $r_{\rm P} = \int d\chi/\cosh\chi$. The resulting Penrose coordinates for de Sitter space are

$$t_{\rm P} = \psi = t_{\rm s}/r_{\rm H} \ , \tag{10.164a}$$

$$r_{\rm P} = \tan^{-1}(\sinh\chi) = r^*_{\rm s}/r_{\rm H} \ , \tag{10.164b}$$

where $r^*_{\rm s}$ is the tortoise radial coordinate

$$r^*_{\rm s} \equiv \int \frac{dr_{\rm s}}{1 + r_{\rm s}^2/r_{\rm H}^2} = r_{\rm H} \tan^{-1}(r_{\rm s}/r_{\rm H}) \ . \tag{10.165}$$

Thus, for anti de Sitter, lines of constant time $t_{\rm s}$ and radius $r_{\rm s}$ in the stationary metric (10.144) correspond also to lines of constant Penrose time and radius $t_{\rm P}$ and $r_{\rm P}$.

The thick (pink) null lines in the Penrose diagram 10.17 outline the causal diamonds of comoving observers

in the open FLRW (10.161) form of the anti de Sitter metric. The null lines also outline the causal wedges of Rindler observers in the Rindler (10.163) form of the anti de Sitter metric.

The horizontal and vertical contours in the Penrose diagram 10.17 are lines of constant ψ and χ in both the open FLRW (10.161) and Rindler (10.163) forms of the anti de Sitter metric. In the open FLRW causal diamonds, the horizontal lines are lines of constant cosmic time ψ, while the vertical contours are geodesics, lines of constant χ. In the Rindler causal wedges, the horizontal contours are lines of constant boost angle χ, while the vertical contours are worldlines of Rindler observers, lines of constant ψ.

Anti de Sitter space is symmetric under boosts in the v–x plane, corresponding to translations of the coordinate χ in either of the open FLRW (10.161) or Rindler (10.163) forms of the anti de Sitter metric. The contours in the Penrose diagram 10.17 are uniformly spaced in χ by 0.4 so as to manifest this symmetry. A similarly symmetric appearance for the ψ coordinate is achieved by choosing contours to be uniformly spaced by 0.4 in the tortoise coordinate ψ^*

$$\psi^* \equiv \begin{cases} \displaystyle\int \frac{d\psi}{\sin\psi} = \ln\tan(\psi/2) & \text{open} \ , \\ \displaystyle\int \frac{d\psi}{\sinh\psi} = \ln\tanh(\psi/2) & \text{Rindler} \ . \end{cases} \tag{10.166}$$

Exercise 10.21 Maximally symmetric spaces.

1. Argue that in a stationary spacetime, every scalar quantity must be independent of time. In particular, the Riemann scalar R, and the contracted Ricci product $R^{\mu\nu}R_{\mu\nu}$ must be independent of time. Conclude that the density ρ and pressure p of a stationary FLRW spacetime must be constant.
2. Conclude that a stationary FLRW spacetime may have curvature and a cosmological constant, but no other source. Show that the FLRW metric then takes the form (10.26) with cosmic scale factor

$$a(t) = \begin{cases} H_0 t & \Omega_k = 1 \ , \ \Omega_\Lambda = 0 \ , \\ \exp(H_0 t) & \Omega_k = 0 \ , \ \Omega_\Lambda = 1 \ , \\ \sqrt{-\Omega_k/\Omega_\Lambda}\,\cosh(\sqrt{\Omega_\Lambda}H_0 t) & \Omega_k < 0 \ , \ \Omega_\Lambda > 0 \ , \\ \sqrt{\Omega_k/\Omega_\Lambda}\,\sinh(\sqrt{\Omega_\Lambda}H_0 t) & \Omega_k > 0 \ , \ \Omega_\Lambda > 0 \ , \\ \sqrt{-\Omega_k/\Omega_\Lambda}\,\sin(\sqrt{-\Omega_\Lambda}H_0 t) & \Omega_k > 0 \ , \ \Omega_\Lambda < 0 \ , \end{cases} \tag{10.167}$$

   with

$$\Omega_\Lambda H_0^2 = \tfrac{1}{3}\Lambda \ , \quad \Omega_k H_0^2 = -\kappa \ . \tag{10.168}$$

   As elsewhere in this chapter, $H = H_0$ at $a = 1$, and the Ω's sum to unity, $\Omega_k + \Omega_\Lambda = 1$.
3. Show that the FLRW metric transforms into the explicitly stationary form (10.144) under a coordinate

transformation to proper radius $r_\mathrm{s} = a(t)x$ and stationary time t_s given by

$$t_\mathrm{s} = \begin{cases} \sqrt{1-\kappa x^2}\; t & \Omega_k = 1\ ,\ \Omega_\Lambda = 0\ , \\ t - \dfrac{1}{H_0}\ln\sqrt{1-H_0^2 r_\mathrm{s}^2} & \Omega_k = 0\ ,\ \Omega_\Lambda = 1\ , \\ \dfrac{1}{\sqrt{\Omega_\Lambda}H_0}\mathrm{acoth}\left[\sqrt{1-\kappa x^2}\,\coth\left(\sqrt{\Omega_\Lambda}H_0 t\right)\right] & \Omega_k < 0\ ,\ \Omega_\Lambda > 0\ , \\ \dfrac{1}{\sqrt{\Omega_\Lambda}H_0}\mathrm{atanh}\left[\sqrt{1-\kappa x^2}\,\tanh\left(\sqrt{\Omega_\Lambda}H_0 t\right)\right] & \Omega_k > 0\ ,\ \Omega_\Lambda > 0\ , \\ \dfrac{1}{\sqrt{-\Omega_\Lambda}H_0}\mathrm{atan}\left[\sqrt{1-\kappa x^2}\,\tan\left(\sqrt{-\Omega_\Lambda}H_0 t\right)\right] & \Omega_k > 0\ ,\ \Omega_\Lambda < 0\ . \end{cases} \tag{10.169}$$

Note that in all cases $t_\mathrm{s} = t$ at the origin $r_\mathrm{s} = 0$.

Concept question 10.22 Milne Universe. In Exercise 10.21 you found that the FLRW metric for an open universe with zero energy-momentum content ($\Omega_k = 1$, $\Omega_\Lambda = 0$), also known as the Milne metric, is equivalent to flat Minkowski space. How can an open universe be equivalent to flat space? Draw a spacetime diagram of Minkowski space showing (a) worldlines of observers at constant comoving FLRW position x, and (b) hypersurfaces of constant FLRW time t.

Concept question 10.23 Stationary FLRW metrics with different curvature constants describe the same spacetime. How can it be that stationary FLRW metrics with different curvature constants κ (but the same cosmological constant Λ) describe the same spacetime?